

# LANG-PINN: FROM LANGUAGE TO PHYSICS-INFORMED NEURAL NETWORKS VIA A MULTI-AGENT FRAMEWORK

Xin He<sup>1</sup>, Liangliang You<sup>3</sup>, Hongduan Tian<sup>2</sup>, Bo Han<sup>2</sup>, Ivor Tsang<sup>1</sup>, Yew-Soon Ong<sup>1</sup>

<sup>1</sup>Agency for Science, Technology and Research (A\*STAR), Singapore

<sup>2</sup>Hong Kong Baptist University, Hong Kong SAR

<sup>3</sup>North China Electric Power University, China

## ABSTRACT

Physics-informed neural networks (PINNs) provide a powerful approach for solving partial differential equations (PDEs), but constructing a usable PINN remains labor-intensive and error-prone. Scientists must interpret problems as PDE formulations, design architectures and loss functions, and implement stable training pipelines. Existing large language model (LLM) approaches address isolated steps such as code generation or architecture suggestion, but typically assume a formal PDE is already specified and therefore lack an end-to-end perspective. We present **Lang-PINN**, an LLM-driven multi-agent system that builds trainable PINNs directly from natural language task descriptions. **Lang-PINN** coordinates four complementary agents: a *PDE Agent* that parses task descriptions into symbolic PDEs, a *PINN Agent* that selects architectures, a *Code Agent* that generates modular implementations, and a *Feedback Agent* that executes and diagnoses errors for iterative refinement. This design transforms informal task statements into executable and verifiable PINN code. Experiments show that **Lang-PINN** achieves substantially lower errors and greater robustness than competitive baselines: mean squared error (MSE) is reduced by up to 3–5 orders of magnitude, end-to-end execution success improves by more than 50%, and reduces time overhead by up to 74%.

## 1 INTRODUCTION

Partial differential equations (PDEs) are central to scientific computing, underpinning applications in physics, engineering, and materials science. Physics-informed neural networks (PINNs) (26) embed governing equations into trainable neural models, providing a unified framework for forward, inverse, and data-scarce problems (12; 22). Despite their promise, training PINNs remains highly challenging, due to gradient pathologies (36), ill-conditioning from the neural tangent kernel perspective (37), failure modes in complex regimes (13), and sensitivity to activation functions, sampling, and decomposition strategies (10; 46; 42; 30; 9). Although libraries and benchmarks such as DeepXDE (22), PINNacle (7), and PDEBench (34) have been developed, deploying a trainable PINN still requires expert-level manual effort in PDE specification, architecture design, and optimization tuning. Efforts to reduce this burden remain fragmented. Traditional automation focuses on hyperparameter search (32; 16; 6; 8) or architecture variants (30; 40; 39), but these approaches assume that the governing PDE has already been written down in an explicit and computationally usable form. Recent progress in large language models (LLMs) enables natural-language interfaces to computational tools, including code generation (27; 17; 21) and multi-step reasoning (45; 29; 23; 38; 41). Domain-specific prototypes such as CodePDE (18) and PINNsAgent (43) demonstrate the feasibility of LLM-driven PDE solvers, but still require manually defined PDE schemas or provide limited verification and iterative refinement. As a result, current automation begins only after the PDE has been fully specified and offers no assistance in constructing the equation itself.

This limitation is substantial, as designing or revising a PDE is often the most technically demanding part of developing a PINN, requiring precise reasoning about operators, coefficients, and boundary or initial conditions, whereas describing changes in the scientific setting using natural language is

straightforward. For example, stating that “the heat source is moved from the center of the domain to the boundary” is simple in text, yet it alters the source term, boundary conditions, and spatial dependence of the governing equation. This mismatch exposes a clear gap: existing systems lack a mechanism for translating natural-language descriptions into fully specified equations for PINN training, motivating automated text-to-PDE construction.

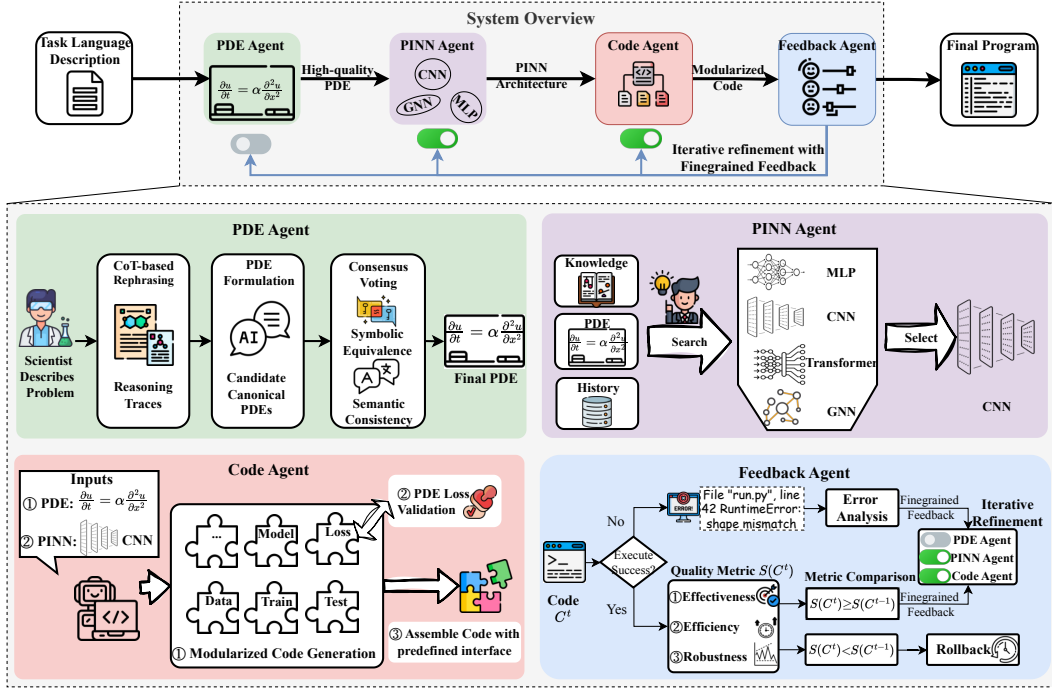


**Figure 1:** System overview of **Lang-PINN**. The framework decomposes end-to-end PINN design into four agents: *PDE Agent* (canonical PDE formulation), *PINN Agent* (training-free architecture selection), *Code Agent* (modularized code generation), and *Feedback Agent* (multi-dimensional evaluation and error analysis).

To address this gap, we propose a multi-agent framework, namely **Lang-PINN**, that decomposes the workflow into four cooperating roles, as shown in Fig. 1. The *PDE Agent* formulates natural language into operators, coefficients, and boundary/initial conditions. The *PINN Agent* aligns PDE characteristics, with periodicity, geometric complexity, and multiscale or chaotic dynamics with inductive biases via a requirement vector and utility score. The *Code Agent* generates modular, contract-preserving training code, while the *Feedback Agent* executes the code, monitors residuals and convergence, and iteratively guides corrections. This structured, verifiable pipeline ensures that scientific consistency, executability, and trainability are treated as first-class design goals.

Our contributions are as follows:

- We propose the first framework that starts from natural language task descriptions and automatically produces complete PINN solutions, including PDE formulation, architecture selection, code generation, and feedback-driven refinement, lowering the entry barrier for domain scientists.
- We construct a benchmark that pairs four-level difficulty task descriptions with ground-truth PDEs, enabling systematic evaluation of semantic-to-symbol grounding and supporting reproducible PINN design.
- We demonstrate substantial improvements across diverse PDEs, reducing mean squared error by up to *3–5 orders of magnitude*, increasing code executability success rates by more than *50%*, and reducing time overhead up to *74%* compared to strong agent-based baselines.

## 2 RELATED WORK

**Physics-Informed Neural Networks.** Physics-Informed Neural Networks (PINNs) (26) integrate governing equations into neural training by penalizing PDE residuals and boundary violations. Numerous variants improve convergence and accuracy, but still rely on expert-specified PDE formula-

tions, architectures, and loss terms. (10; 46; 22; 42; 30; 9) Yet, these approaches still require experts to manually specify PDE formulations, architectures, and loss terms. Our work instead seeks to automate these design choices from task descriptions.

**LLM Agents and Reasoning Strategies.** Large language and code models have enabled text-to-code generation (27; 17) and agentic software engineering (11; 44). In scientific domains, CodePDE (18) shows that inference-time reasoning and self-debugging can generate PDE solvers from text. Prompting strategies such as SCoT (15) and Self-Debug (3) further improve reasoning consistency. However, these approaches remain single-agent and lack physics-grounded validation, limiting their applicability to scientific surrogates. Our framework extends this direction by coupling reasoning and feedback across multiple specialized agents for PINNs.

**Automated PINN Design.** Classical Automated Machine Learning (AutoML) methods (8), including Bayesian optimization (32), Hyperband (16), and BOHB (6), aim to reduce manual effort in tuning architectures and hyperparameters. Applied to physics-informed settings, however, they struggle with residual imbalance, unit inconsistency, and multi-scale stiffness, often requiring expert intervention. Recent PINN-oriented searches (36; 42) mitigate some challenges but still assume human-specified PDEs and loss structures. In contrast, our approach introduces a dedicated multi-agent system for PINN automation, integrating PDE translation, architecture design, and feedback-driven refinement to minimize manual design effort and achieve end-to-end trainability.

### 3 AN INVESTIGATION ON MODULES OF PINNS

Despite recent progress concentrating on PDE parsing and PINN architecture search, the properties of modules in PINNs remain under-explored. Since the goal of this paper is to build an end-to-end automated PINN pipeline, it is crucial to understand these modules comprehensively. Accordingly, we empirically analyze three pivotal modules, PDE parsing, architecture curation, and code generation, these show that existing PINN pipelines suffer from three practical bottlenecks: problem formulation linguistic variability, model performance variability, and code generation complexity.

#### 3.1 LINGUISTIC VARIABILITY OF TASK FORMULATION FROM TEXTUAL DESCRIPTION TO PDEs

Typically, a PINN pipeline begins with translating natural-language descriptions into formal PDEs. In the generated PDEs, the loss terms are defined, the solution space is constrained, and all downstream stages are conditioned. As the foundation of the entire pipeline, any error in this step invalidates the pipeline. Thus, it is essential to formulate the PDEs in a reliable way.

In this section, we propose to determine the significance of the reliable PDE formulation. Specifically, we propose a tiny augmented dataset, *Task2PDE*, where eight examples are randomly sampled from PINNacle benchmark (7) and re-expressed with four levels of linguistic variability. Details about re-expression are available in Appendix 4. In this way, each sample is paired with 50 descriptions for each level of variability, yielding 1,600 description-PDE pairs. We adopt four popular open-source LLMs (Llama2 (35), Vicuna (4), DeepSeek-V3 (5), Qwen (1)) and evaluate them with *symbolic equivalence* over the *Task2PDE* dataset. Results in Fig. 2 show that symbolic accuracy declines steadily as the linguistic variability of the descriptions increases, indicating that even small shifts in wording can substantially alter the PDE inferred by an LLM and undermine the reliability of the formulation.

Although symbolic equivalence is mathematically precise, it is brittle for natural-language-derived PDEs, where equivalent terms and benign coefficient variations are misclassified, indicating that symbolic matching alone is insufficient under noisy or stylistically diverse inputs. This motivates

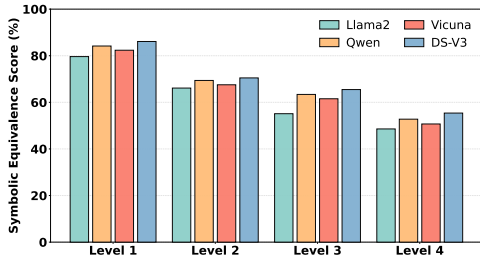


**Figure 2:** Impact of linguistic variability on PDE translation. Accuracy is reported across four levels of description difficulty using symbolic equivalence.

the *PDE Agent* (Sec. 4.2), which augments symbolic checks with semantic evaluation and consensus voting while retaining symbolic verification as a final safeguard.

### 3.2 VARIABILITY OF ARCHITECTURE PERFORMANCE ACROSS PDES

Once the PDE is specified, selecting a suitable PINN architecture is crucial. The inductive bias of the network, such as its preference for local patterns, long-range dependencies, or structural constraints, directly affects stability and accuracy. A poor match can lead to slow convergence or large residual errors. To demonstrate this effect, we benchmark four representative architectures (MLP, CNN, GNN, and Transformer) on PDEs including Shallow Water, Convection, Poisson, and Heat. As shown in Fig. 3, performance varies markedly across PDEs. CNNs and Transformers excel on Convection and Heat,

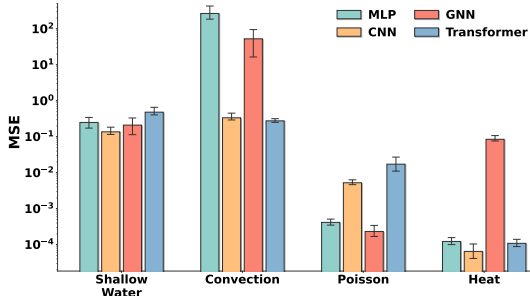
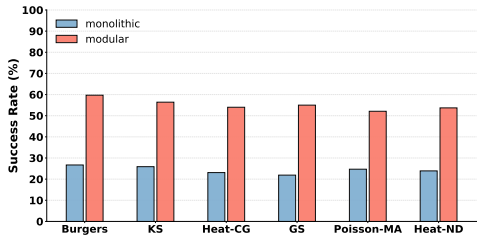


**Figure 3:** Comparative MSE of PINN architectures on representative PDEs. CNNs and Transformers excel on Convection and Heat, while MLPs and GNNs achieve the lowest error on Poisson. For Shallow Water, differences are minor. These results show that no single architecture is universally effective, motivating approaches that adapt PINN designs to the operators and structures of different PDEs.

### 3.3 COMPLEXITY OF CODE GENERATION IN END-TO-END WORKFLOWS

After the PDE and PINN architecture are specified, the next step is to generate executable code, including model definitions, physics-informed losses, data pipelines, and training routines. This process is complex because multiple components must not only be correct in isolation but also interact reliably, making executability a central challenge.



To study code generation paradigms, we compare *monolithic generation*, where an LLM produces the entire pipeline in a single pass, with *modular generation*, where code is synthesized by components. As shown in Fig. 4, modular generation consistently achieves more than twice the success rate of monolithic generation across six representative PDEs (Burgers, KS, Heat-CG, GS, Poisson-MA, Heat-ND). The modular design localizes errors, preserves correct components, and avoids regenerating the full script, thereby substantially improving executability. These results motivate the design of the **Code Agent**, which adopts the modular paradigm. We note that this experiment isolates the effect of modularization alone; when combined with the **Feedback Agent** in our full framework, success rates improve even further, as shown in later sections.

**Figure 4:** Comparative Success Rate(%) of different code generation paradigm (monolithic vs. modular) on six PDEs.

## 4 METHOD

### 4.1 SYSTEM OVERVIEW

According to the analyses in the previous section, we observe that end-to-end PINN automation breaks down due to cascading dependencies: minor linguistic variations in PDE formulation propagate into architecture mismatches, and monolithic code generation further amplifies upstream errors. Thus, in this section, we propose to construct an end-to-end automated PINN framework to enhance verification and reliability.

Fig. 1 presents **Lang-PINN**, our multi-agent framework that converts natural-language task descriptions into executable PINN training code. It consists of four agents with distinct roles: the *PDE Agent* formalizes task descriptions into governing equations, the *PINN Agent* selects suitable architectures, the *Code Agent* generates modular implementations, and the *Feedback Agent* executes and evaluates outputs. These agents interact in a sequential workflow, with the *Feedback Agent*

providing iterative diagnostics that refine earlier stages, particularly code generation. This modular and feedback-driven design reduces error propagation and ensures reliable, scientifically valid PINN implementations.

## 4.2 PDE AGENT

To alleviate the sensitivity to linguistic variability identified in Sec. 3.1, the *PDE Agent* uses a label-free reasoning–selection pipeline. Given a task description  $d$ , the agent samples  $K$  chain-of-thought (CoT) trajectories, cleans each trajectory into a normalized description  $\hat{d}_k$ , and formulates a canonical PDE candidate  $E_k$ . Invalid candidates are filtered by template validation (operator well-formedness, residual form, admissible boundary/initial terms). The remaining set  $\mathcal{E} = \{E_1, \dots, E_K\}$  is then resolved via consensus voting, and the agent selects the candidate that is most similar to the others under a joint symbolic–semantic criterion.

**Symbolic Equivalence.** To assess whether two candidate PDEs express the same operator structure, we compute a *symbolic equivalence score* based on their abstract syntax trees (ASTs). Each PDE  $E$  is parsed into a canonical symbolic tree  $\mathcal{T}(E)$  using Sympy, where nodes represent operators (e.g.,  $\partial_t$ ,  $\partial_x^2$ , nonlinear products) and leaves correspond to variables or constants.

Given two trees  $\mathcal{T}(E_i)$  and  $\mathcal{T}(E_j)$ , we define their symbolic equivalence as a normalized tree-matching score,

$$\text{sym}(E_i, E_j) = \frac{|\mathcal{M}(\mathcal{T}(E_i), \mathcal{T}(E_j))|}{\max(|\mathcal{T}(E_i)|, |\mathcal{T}(E_j)|)}, \quad (1)$$

where  $\mathcal{M}(\mathcal{T}(E_i), \mathcal{T}(E_j))$  denotes the set of matched subtrees under operator-preserving alignment, and  $|\mathcal{T}(\cdot)|$  counts the total nodes. This yields a score in  $[0, 1]$ , equal to 1 if two PDEs are symbolically equivalent (identical operator trees) and decreasing smoothly as structural discrepancies grow.

This formulation abstracts our Sympy-based implementation, where equivalence is resolved by recursively comparing operator nodes and their children up to commutativity and normalization rules. It aligns with symbolic regression principles (28; 14), while providing robustness to variations in coefficient presentation or term ordering.

**Semantic Consistency.** Symbolic matching alone cannot capture cases where mathematically equivalent PDEs are expressed in different notations or variable names. Following ideas from mathematical information retrieval (47), we therefore introduce a *semantic consistency score*. Each candidate PDE  $E$  is paraphrased into a normalized summary  $g(E)$  that encodes its domain, operator types, and forcing terms. The semantic consistency between two candidates  $E_i$  and  $E_j$  is then defined as

$$\text{sem}(E_i, E_j) = \sigma(g(E_i), g(E_j)), \quad (2)$$

where  $\sigma$  is a sentence-level similarity function such as embedding cosine similarity or LLM-based entailment scoring. This yields values in  $[0, 1]$  and provides robustness to symbol renaming, coefficient scaling, or algebraic rearrangements that preserve meaning but alter surface form.

**Consensus Voting.** Finally, we combine symbolic and semantic similarities into a composite score  $S(E_i, E_j) = \alpha \text{sym}(E_i, E_j) + (1 - \alpha) \text{sem}(E_i, E_j)$ . Each candidate is then compared against the others, and the one with the highest average similarity is selected as the final PDE. This simple consensus step ensures that the chosen equation is both structurally consistent and semantically faithful to the task description. We use a calibrated similarity threshold of 0.80; details are provided in Appendix 3.4.

## 4.3 PINN AGENT

Different PDEs exhibit distinct sensitivities to network architecture, and no single model is uniformly optimal (Sec. 3.2). The *PINN Agent* selects an appropriate architecture for a newly extracted PDE without any training-time search. Given a canonical PDE representation  $E$ , the agent follows a two-stage process: it first queries a *history cache*  $\mathcal{H}$  to reuse the architecture and hyperparameters of a previously solved, highly similar PDE; if no such entry exists, it performs knowledge-guided matching using a *knowledge base*  $\mathcal{K}$ , which scores architectures by their compatibility with the characteristics of  $E$ . This design enables efficient reuse for recurring PDEs while providing principled generalization to unseen ones.

**History Reuse.** The history cache  $\mathcal{H}$  is an automatically maintained collection of past tasks. Each entry records: 1) the natural-language task description, 2) the extracted PDE together with its feature vector  $\phi(E)$ , and 3) the architecture and hyperparameters that produced the best PINN solution.

**Knowledge-guided Matching.** In the absence of reusable history, the agent applies *knowledge-guided matching* to select architectures based on knowledge base  $\mathcal{K}$ . The key idea is to embed PDEs and architectures into a representation vector, where their alignment can be systematically evaluated. We first describe how PDEs are represented, then how architectures are encoded, and finally how the two are matched.

1. *PDE Feature Representation.* To represent the input side of the matching process, each PDE  $E$  is encoded as a feature vector

$$\phi(E) = [f_1(E), f_2(E), \dots, f_n(E)]^\top, \quad (3)$$

where  $f_i(E)$  denotes a quantifiable physical property, including *periodicity*, *geometry complexity*, and *multi-scale demand*. Periodicity reflects whether domains or boundary conditions repeat, geometry complexity captures whether the domain is structured or irregular, and multi-scale demand indicates the extent of interacting scales or chaotic regimes. Formal definitions are given in Appendix 1. These dimensions are motivated by prior findings that Fourier or sinusoidal layers align with periodic problems (31; 19), graph-based models are effective for irregular geometries (24; 2), and attention or spectral operators handle multi-scale demand, e.g., dynamics (25). We adopt a lightweight and interpretable feature design, as these properties capture the primary factors influencing architecture suitability in our benchmark. Learning richer PDE–architecture embeddings is an interesting direction for future work.

2. *Architecture Capability Representation.* To make architectures comparable with PDE features, each architecture  $\mathcal{A}$  is represented by a capability vector

$$\psi(\mathcal{A}) = [a_1(\mathcal{A}), a_2(\mathcal{A}), \dots, a_n(\mathcal{A})]^\top, \quad (4)$$

where  $a_i(\mathcal{A})$  measures its competence on property  $i$  within PDE feature representation. Capability values are inferred through LLM reasoning and refined with historical experimental outcomes, ensuring adaptability across tasks. Formal definitions are given in Appendix 1.

3. *PDE–Architecture Matching* The compatibility between a PDE  $E$  and an architecture  $\mathcal{A}$  is measured using a weighted cosine similarity:

$$S(\mathcal{A}, E) = \frac{(\mathbf{W}\phi(E))^\top \psi(\mathcal{A})}{\|\mathbf{W}\phi(E)\|_2 \cdot \|\psi(\mathcal{A})\|_2}, \quad (5)$$

where  $\mathbf{W} = \text{diag}(w_{\text{per}}, w_{\text{geo}}, w_{\text{ms}})$  assigns importance weights to each property. In practice, we prioritize multi-scale demand over geometry and periodicity, as mismatches on the former are most detrimental to convergence (19; 24; 2; 31). The final architecture is then selected as

$$\mathcal{A}^* = \arg \max_{\mathcal{A} \in \Theta} S(\mathcal{A} | E). \quad (6)$$

**Architecture Template Instantiation.** After selecting  $\mathcal{A}^*$ , the agent instantiates the model using predefined *architecture templates*. Each template specifies essential architectural parameters (e.g., number of layers, hidden width, activation function, embedding dimension) and training hyperparameters (e.g., learning rate, batch size, optimizer), with fields populated from the configuration stored  $\mathcal{K}$  for  $\mathcal{A}^*$  (or defaults when unavailable). This templated instantiation avoids free-form code generation errors and ensures consistent, reproducible PINN construction across tasks.

The knowledge base  $\mathcal{K}$  does not contain task-specific solutions, but instead encodes general architectural priors commonly reported in the PINN literature (e.g., Fourier representations for periodic problems or graph models for irregular geometries), which guide architecture selection without introducing additional problem-specific information.

#### 4.4 CODE AGENT

Directly prompting an LLM to generate the entire PINN pipeline in one pass often produces brittle code, where model definition, loss formulation, and training loops are tightly coupled. Errors become difficult to isolate, and fixing them typically requires regenerating the whole script. To avoid this, the *Code Agent* adopts a modular strategy with explicit verification mechanisms.

**Modularized code generation.** Instead of producing a monolithic script, the *Code Agent* decomposes the pipeline into independent modules: (i) model definition, (ii) PDE loss, (iii) data pre-processing, (iv) training loop, (v) validation, and (vi) main function. Each module is generated separately, allowing faults to be localized and corrected without regenerating unrelated components.

**Interface constraints.** Modules are connected through standardized input–output formats, ensuring compatibility and composability. This design makes it possible to update or replace one module without introducing inconsistencies elsewhere, thereby reducing correction cost and enabling fine-grained refinement.

**PDE loss verification.** For the PDE loss module, the generated code is parsed back into a symbolic PDE  $\hat{E}$  and checked for equivalence with the PDE  $E$  provided by the *PDE Agent*. Only loss modules that pass this symbolic check are retained, ensuring that the optimization objective faithfully encodes the governing equation.

#### 4.5 FEEDBACK AGENT

The *Feedback Agent* closes the loop by leveraging runtime signals to refine earlier stages. Built on the modular code of the *Code Agent*, it translates execution diagnostics into localized suggestions, avoiding global regeneration and improving reliability.

**Error localization and correction.** When executing the generated code, two scenarios arise. If runtime errors occur, the *Feedback Agent* analyzes the error messages and attributes them to the most likely module (e.g., model structure, loss function, training loop). It then instructs the *Code Agent* to regenerate only the faulty component, avoiding unnecessary changes to other modules. If the issue originates upstream (e.g., in PDE specification or PINN architecture), the *Feedback Agent* can escalate its directive to the corresponding agent, ensuring that corrections are applied at the appropriate level.

**Multi-dimensional quality evaluation.** If execution succeeds, the *Feedback Agent* evaluates the code along three complementary dimensions: (i) *effectiveness*, measured by PDE residual error (e.g., MSE); (ii) *efficiency*, measured by convergence speed and resource cost (steps, FLOPs, parameters); and (iii) *robustness*, measured by loss smoothness and the absence of gradient pathologies. Each metric is normalized, and a weighted sum produces an overall quality score:

$$S(C) = \sum_{i=1}^3 w_i \hat{m}_i(C), \quad (7)$$

where  $C$  denotes the generated code,  $\hat{m}_i$  the normalized value of the  $i$ -th metric, and  $w_i$  its weight. Detailed definitions and quantification of these metrics are provided in Appendix 2.

**Iterative refinement.** The decision to accept or reject a new version is based on comparing the current score  $S(C^{(t)})$  with the previous score  $S(C^{(t-1)})$ . If the new version improves, the agent proceeds; otherwise, it reverts and restarts optimization. By coupling modular generation with runtime feedback, the system ensures that diagnostic signals can be acted upon locally rather than globally, providing fine-grained corrections that improve reliability and efficiency over iterations.

## 5 EXPERIMENTS

### 5.1 EXPERIMENTAL SETTINGS

**Benchmark Datasets** We evaluate **Lang-PINN**, on the PINNacle benchmark (7), which comprises 14 representative PDEs across 1D, 2D, 3D, and ND settings: *Burgers*, *Wave-C*, *KS*, *Burgers-C*, *Wave-CG*, *Heat-CG*, *NS-C*, *GS*, *Heat-MS*, *Heat-VC*, *Poisson-MA*, *Poisson-CG*, *Poisson-ND*, *Heat-ND*. This collection spans diverse dimensionalities, geometric complexities, and dynamical regimes, providing a rigorous testbed for automated PINN design. At the task-to-PDE stage, **Lang-PINN**, operates from natural-language inputs: for each PDE, three distinct textual problem descriptions are constructed and translated into canonical PDE formulations before downstream modeling. In contrast, baseline methods are directly provided with the canonical PDE formulations from the benchmark, as they cannot perform this translation step. For fairness, all quantitative metrics are

computed solely on the resulting PINN performance, independent of whether the PDE was inferred or given. Each task is evaluated over 10 independent runs, with up to three refinement iterations per run, ensuring fairness across methods and robustness to stochasticity.

**Baselines** We include **PINNacle** (7) as a non-agent reference that fixes both PDEs and architectures and directly trains PINNs. All other baselines adopt LLM-based agents but still assume the PDE and architecture are given. **RandomAgent** and **BayesianAgent** explore architectures through random or Bayesian search with error-only feedback, while **SCoT** (15) and **Self-Debug** (3) rely on prompting to generate losses or partial code, without full feedback or PDE formulation. **PINNsAgent** (43) can generate code and refine it based on execution results, but it still has limitations. It cannot automatically formulate PDEs from physical descriptions, nor can it split a large problem into smaller tasks for multiple agents to handle independently. Instead, it relies on a user-provided PDE to begin the process. As summarized in Table 1, none of these baselines support PDE formulation, code generation is at best partial, and feedback is limited to error detection, whereas **Lang-PINN** spans all dimensions in a coordinated multi-agent system. For fair comparison, we adopt Deepseek-V3 (5) (top-p=0.9, temperature=0.2, max\_tokens=2048) as the LLM backbone for all agent-based baselines and Lang-PINN.

**Metrics** The **success rate** measures robustness as the proportion of runs whose generated code executes end-to-end without runtime errors, independent of training accuracy. The **mean squared error (MSE)** quantifies numerical fidelity of the PINN solution. The **iterations to a successful run** report the number of refinement cycles required to obtain the first runnable version, reflecting convergence speed. The **end-to-end time cost** records the wall-clock time from pipeline start to the first executable program, characterizing practical efficiency. All results are averaged over 10 runs with up to 30 refinement cycles per run.

Method	PF	AD	CG	FS
PINNacle	×	×	×	×
RandomAgent	×	✓	Partial	×
BayesianAgent	×	✓	Partial	×
SCoT	×	×	Partial	×
Self-Debug	×	×	Partial	Err-only
PINNsAgent	×	✓	Full	Err+Metrics
<b>Lang-PINN</b>	✓	✓	Full	Err+Metrics

**Table 1:** Comparison of methods across five functional dimensions: **PF** (PDE formulation), **AD** (architecture design), **CG** (code generation), and **FS** (feedback signal). For **FS**, “Err+Metrics” augments runtime error with validation metrics.

## 5.2 MAIN RESULTS

**Table 2:** Comparative performance (MSE) on 14 different PDEs (averaged over 10 runs).

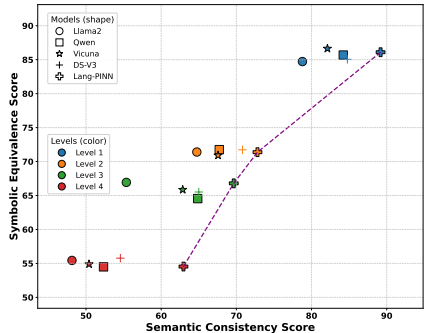
Dim	PDE	RandomAgent	BayesianAgent	PINNsAgent	SCoT	Self-Debug	Ours	PINNacle
1D	Burgers	6.63E-02	8.70E-02	1.10E-04	1.40E+01	1.26E+01	<b>6.48E-05</b>	7.90E-05
	Wave-C	1.50E-01	1.78E-01	3.74E-02	1.28E+00	1.18E+00	<b>2.25E-03</b>	3.01E-03
	KS	1.09E+00	1.10E+00	1.09E+00	3.33E+00	2.93E+00	<b>1.62E-03</b>	1.04E+00
2D	Burgers-C	2.48E-01	2.42E-01	2.93E-01	4.54E-01	4.09E-02	<b>2.88E-03</b>	1.09E-01
	Wave-CG	2.87E-02	2.11E-02	4.59E-02	2.00E+00	1.90E+00	<b>2.52E-03</b>	2.99E-02
	Heat-CG	3.96E-01	1.17E-01	9.06E-02	4.38E+00	3.81E-02	<b>1.35E-03</b>	8.53E-04
	NS-C	4.02E-03	5.12E-03	<b>1.40E-05</b>	5.67E-01	5.27E-01	4.05E-05	2.33E-05
	GS	4.28E-03	4.03E-03	3.37E+08	3.76E+00	3.35E+00	<b>1.89E-03</b>	4.32E-03
	Heat-MS	1.84E-02	7.48E-03	1.06E-04	7.10E-02	6.04E-03	<b>2.27E-05</b>	5.27E-05
	Heat-VC	3.57E-02	3.93E-02	1.43E-02	4.46E+00	4.01E-02	<b>1.62E-03</b>	1.76E-03
Poisson-MA	5.87E+00	5.82E+00	3.16E+00	1.24E+04	1.07E+04	<b>2.25E-03</b>	1.83E+00	
3D	Poisson-CG	3.82E-02	2.55E-02	3.35E-02	4.17E-02	9.51E-03	<b>1.35E-03</b>	9.51E-04
	Poisson-ND	1.30E-04	4.72E-05	4.77E-04	9.93E+00	9.43E+00	<b>8.42E-06</b>	2.09E-06
ND	Heat-ND	2.58E-00	<b>1.18E-04</b>	8.57E-04	3.74E+00	3.40E-03	4.72E-04	8.52E+00

Table 2 shows that **Lang-PINN** achieves the lowest errors on most PDEs, despite being the only approach that must first infer PDE formulations from natural-language descriptions. In contrast, *PINNacle* is a human-expert-designed reference with fixed governing PDEs and PINN architectures; even against this strong baseline, **Lang-PINN** delivers significant improvements, reducing errors on *KS* (1D), *Poisson-MA* (2D), and *Heat-ND* (ND) by over three orders of magnitude. Compared to agent-based baselines, whose errors on *KS* and *Poisson-MA* remain around  $10^0$  to  $10^4$ , Lang-PINN reaches  $10^{-3}$ , demonstrating substantially stronger solution fidelity.

Fig. 5 further reports that **Lang-PINN** consistently delivers the highest reliability, with success exceeding 80% in 1D and 2D regimes where baselines such as RandomAgent, BayesianAgent, and PINNsAgent typically remain below 35%, and remaining robust in 3D with success rates close to 75%. In terms of efficiency, with all methods capped at 50 iterations, **Lang-PINN** converges in only 8 iterations on average which is about 74% fewer than the worst baseline (31), and consistently reduces iteration counts compared to BayesianAgent (29), PINNsAgent (21), SCoT (17), and Self-Debug (14). Finally, as shown in Appendix 3.5, **Lang-PINN** reduces end-to-end PDE-solving time by about 21%–52% compared with all baselines.

### 5.3 ABLATION STUDIES

**The Impact of PDE Agent.** Since Sec. 3.1 highlights the difficulty of grounding natural-language descriptions into PDEs, we conduct an ablation study to assess the contribution of the PDE Agent. Fig. 6 shows translation accuracy under increasing linguistic complexity. While all baselines degrade sharply from Level1 to Level4, our full agent achieves the highest semantic consistency with competitive symbolic equivalence. Gains are most evident under noisy and fragmented settings, where reasoning, canonicalization, validation, and self-consistency selection stabilize outputs, demonstrating robust task-to-equation translation.



**Figure 6:** PDE formulation accuracy across different linguistic complexity. **Lang-PINN** lies on the Pareto frontier, balancing symbolic equivalence and semantic consistency.

**The Impact of PINN Agent.** To evaluate the contribution of the *PINN Agent* in architecture selection, we compare it with a fixed-MLP variant across all PDEs, with only depth and width tuned. In contrast, the *PINN Agent* leverages PDE, prior knowledge, and history to select among architecture families (MLP, CNN, GNN, and Transformer). As shown in Fig. 7, dynamic selection achieves substantially lower MSEs across 14 PDEs, with the largest gains on periodic, irregular, or multi-scale problems (KS, Poisson-MA, Heat-ND), highlighting the importance of adaptive architecture selection for PDE-aware generalization.

**The Impact of Code Agent.** We compare the Code Agent’s modular code generation paradigm with a monolithic generator that produces the entire code in one pass. In the monolithic setting, runtime errors are difficult to localize and require regenerating the full script, leading to fragile execution. By contrast, the Code Agent decomposes the pipeline into modules (model, loss, training loop), enabling localized correction and reuse. As shown in Fig. 8, this modular design improves execution success rates by over 20% across PDEs, highlighting its role in executability.

**The Impact of Feedback Agent.** We compare error-only feedback with our full design, which augments execution errors with the multi-dimensional quality metrics introduced in Sec. 4.5, including loss smoothness, gradient stability, and convergence behavior. As shown in Fig. 9, these additional metrics consistently reduce MSE across PDE benchmarks, in some cases by several orders of magnitude, confirming that metric-guided feedback is critical for improving accuracy once executability is secured.

## 6 CONCLUSION

**Lang-PINN** constructs PINNs from task descriptions by integrating PDE parsing, architecture selection, modular code generation, and feedback refinement. Compared to baselines, **Lang-PINN** achieves lower errors,

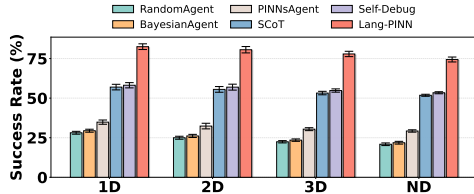


**Figure 5:** Comparative success rates (%) of different methods for generating executable PINNs across 1D, 2D, 3D, and ND PDEs.

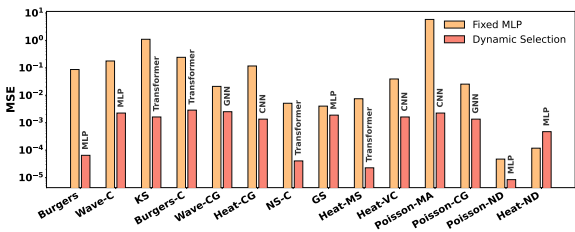


**Figure 7:** Ablation study of the PINN Agent: the fixed MLP variant (yellow) uses the same MLP backbone for all PDEs, while the full PINN Agent (red) dynamically selects among candidate architectures (e.g., MLP, CNN, and GNN). Dynamic selection consistently reduces MSE across 14 PDEs, demonstrating the effectiveness of adaptive architecture design.

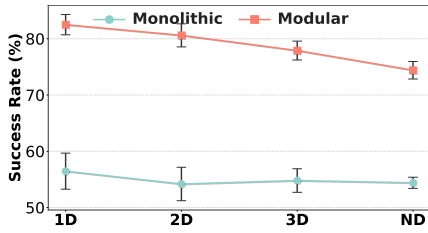


**Figure 8:** Ablation on the *Code Agent*: success rate (%) of monolithic versus modular code generation.

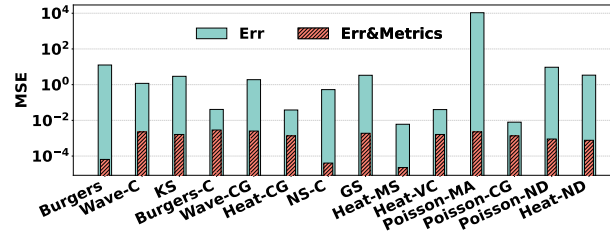


**Figure 9:** Ablation on the *Feedback Agent*: MSE comparison of error-only feedback (*Err*) vs. error feedback augmented with code quality metrics (*Err&Metrics*).

higher execution success rates, and significantly reduced time overhead, highlighting LLM-based agents’ potential to bridge scientific intent and executable models.

## ETHICS STATEMENT

This work does not involve human subjects, sensitive personal data, or experiments that could raise ethical concerns. The datasets used are publicly available, and no privacy or security issues are implicated. Our study focuses purely on methodological and computational aspects, and therefore we do not anticipate any direct ethical or societal risks arising from this research.

## REPRODUCIBILITY STATEMENT

We have made extensive efforts to ensure the reproducibility of our results. The descriptions of the proposed models and algorithms are included in the main text, while additional implementation details, hyperparameter settings, and training procedures are provided in the appendix and supplementary material. Information about datasets and data preprocessing steps is clearly documented. To further facilitate reproducibility, we provide an anonymous repository containing the source code, experiment scripts, and configuration files in the supplementary materials.

## THE USE OF LARGE LANGUAGE MODELS

In preparing this manuscript, we used LLM to refine the clarity, fluency, and readability of the English writing. The LLM was employed only for linguistic polishing and expression improvement. All scientific content, analysis, results, and conclusions were conceived, validated, and written by the authors. The authors take full responsibility for the accuracy and integrity of the scientific claims presented in this paper.

## REFERENCES

- [1] Jinze Bai, Shuai Bai, Yunfei Chu, Zeyu Cui, Kai Dang, Xiaodong Deng, Yang Fan, Wenbin Ge, Yu Han, Fei Huang, Binyuan Hui, Luo Ji, Mei Li, Junyang Lin, Runji Lin, Dayiheng Liu, Gao Liu, Chengqiang Lu, Keming Lu, Jianxin Ma, Rui Men, Xingzhang Ren, Xuancheng Ren, Chuanqi Tan, Sinan Tan, Jianhong Tu, Peng Wang, Shijie Wang, Wei Wang, Shengguang Wu, Benfeng Xu, Jin Xu, An Yang, Hao Yang, Jian Yang, Shusheng Yang, Yang Yao, Bowen Yu, Hongyi Yuan, Zheng Yuan, Jianwei Zhang, Xingxuan Zhang, Yichang Zhang, Zhenru Zhang, Chang Zhou, Jingren Zhou, Xiaohuan Zhou, and Tianhang Zhu. Qwen technical report, 2023.
- [2] Johannes Brandstetter, Daniel Worrall, and Max Welling. Message passing neural pde solvers. *arXiv preprint arXiv:2202.03376*, 2022.
- [3] Xinyun Chen, Maxwell Lin, Nathanael Schärli, and Denny Zhou. Teaching large language models to self-debug. *arXiv preprint arXiv:2304.05128*, 2023.
- [4] Wei-Lin Chiang, Zhuohan Li, Zi Lin, Ying Sheng, Zhanghao Wu, Hao Zhang, Lianmin Zheng, Siyuan Zhuang, Yonghao Zhuang, Joseph E. Gonzalez, Ion Stoica, and Eric P. Xing. Vicuna: An open-source chatbot impressing gpt-4 with 90%\* chatgpt quality, March 2023.
- [5] DeepSeek-AI, Aixin Liu, Bei Feng, Bing Xue, Bingxuan Wang, Bochao Wu, Chengda Lu, Chenggang Zhao, Chengqi Deng, Chenyu Zhang, Chong Ruan, Damai Dai, Daya Guo, Dejian Yang, Deli Chen, Dongjie Ji, Erhang Li, Fangyun Lin, Fucong Dai, Fuli Luo, Guangbo Hao, Guanting Chen, Guowei Li, H. Zhang, Han Bao, Hanwei Xu, Haocheng Wang, Haowei Zhang, Honghui Ding, Huajian Xin, Huazuo Gao, Hui Li, Hui Qu, J. L. Cai, Jian Liang, Jianzhong Guo, Jiaqi Ni, Jiashi Li, Jiawei Wang, Jin Chen, Jingchang Chen, Jingyang Yuan, Junjie Qiu, Junlong Li, Junxiao Song, Kai Dong, Kai Hu, Kaige Gao, Kang Guan, Kexin Huang, Kuai Yu, Lean Wang, Lecong Zhang, Lei Xu, Leyi Xia, Liang Zhao, Litong Wang, Liyue Zhang, Meng Li, Miaojun Wang, Mingchuan Zhang, Minghua Zhang, Minghui Tang, Mingming Li, Ning Tian, Panpan Huang, Peiyi Wang, Peng Zhang, Qiancheng Wang, Qihao Zhu, Qinyu Chen, Qiushi Du, R. J. Chen, R. L. Jin, Ruiqi Ge, Ruisong Zhang, Ruizhe Pan, Runji Wang, Runxin Xu, Ruoyu Zhang, Ruyi Chen, S. S. Li, Shanghao Lu, Shangyan Zhou, Shanhuang Chen, Shaoqing Wu, Shengfeng Ye, Shengfeng Ye, Shirong Ma, Shiyu Wang, Shuang Zhou, Shuiping Yu, Shunfeng Zhou, Shuting Pan, T. Wang, Tao Yun, Tian Pei, Tianyu Sun, W. L. Xiao, Wangding Zeng, Wanbiao Zhao, Wei An, Wen Liu, Wenfeng Liang, Wenjun Gao, Wenqin Yu, Wentao Zhang, X. Q. Li, Xiangyue Jin, Xianzu Wang, Xiao Bi, Xiaodong Liu, Xiaohan Wang, Xiaojin Shen, Xiaokang Chen, Xiaokang Zhang, Xiaosha Chen, Xiaotao Nie, Xiaowen Sun, Xiaoxiang Wang, Xin Cheng, Xin Liu, Xin Xie, Xingchao Liu, Xingkai Yu, Xinnan Song, Xinxia Shan, Xinyi Zhou, Xinyu Yang, Xinyuan Li, Xuecheng Su, Xuheng Lin, Y. K. Li, Y. Q. Wang, Y. X. Wei, Y. X. Zhu, Yang Zhang, Yanhong Xu, Yanhong Xu, Yanping Huang, Yao Li, Yao Zhao, Yaofeng Sun, Yaohui Li, Yaohui Wang, Yi Yu, Yi Zheng, Yichao Zhang, Yifan Shi, Yiliang Xiong, Ying He, Ying Tang, Yishi Piao, Yisong Wang, Yixuan Tan, Yiyang Ma, Yiyuan Liu, Yongqiang

- Guo, Yu Wu, Yuan Ou, Yuchen Zhu, Yudian Wang, Yue Gong, Yuheng Zou, Yujia He, Yukun Zha, Yunfan Xiong, Yunxian Ma, Yuting Yan, Yuxiang Luo, Yuxiang You, Yuxuan Liu, Yuyang Zhou, Z. F. Wu, Z. Z. Ren, Zehui Ren, Zhangli Sha, Zhe Fu, Zhean Xu, Zhen Huang, Zhen Zhang, Zhenda Xie, Zhengyan Zhang, Zhewen Hao, Zhibin Gou, Zhicheng Ma, Zhigang Yan, Zhihong Shao, Zhipeng Xu, Zhiyu Wu, Zhongyu Zhang, Zhuoshu Li, Zihui Gu, Zijia Zhu, Zijun Liu, Zilin Li, Ziwei Xie, Ziyang Song, Ziyi Gao, and Zizheng Pan. Deepseek-v3 technical report, 2025.
- [6] Stefan Falkner, Aaron Klein, and Frank Hutter. Bohb: Robust and efficient hyperparameter optimization at scale. In *International conference on machine learning*, pages 1437–1446. PMLR, 2018.
- [7] Zhongkai Hao, Jiachen Yao, Chang Su, Hang Su, Ziao Wang, Fanzhi Lu, Zeyu Xia, Yichi Zhang, Songming Liu, Lu Lu, and Jun Zhu. Pinnacle: A comprehensive benchmark of physics-informed neural networks for solving pdes, 2023.
- [8] Xin He, Kaiyong Zhao, and Xiaowen Chu. Automl: A survey of the state-of-the-art. *Knowledge-Based Systems*, 212:106622, 2021.
- [9] Ameya D Jagtap and George Em Karniadakis. Extended physics-informed neural networks (xpinnns): A generalized space-time domain decomposition based deep learning framework for nonlinear partial differential equations. *Communications in Computational Physics*, 28(5), 2020.
- [10] Ameya D Jagtap, Kenji Kawaguchi, and George Em Karniadakis. Adaptive activation functions accelerate convergence in deep and physics-informed neural networks. *Journal of Computational Physics*, 404:109136, 2020.
- [11] Carlos E Jimenez, John Yang, Alexander Wettig, Shunyu Yao, Kexin Pei, Ofir Press, and Karthik Narasimhan. Swe-bench: Can language models resolve real-world github issues? *arXiv preprint arXiv:2310.06770*, 2023.
- [12] George Em Karniadakis, Ioannis G. Kevrekidis, Lu Lu, Paris Perdikaris, Sifan Wang, and Liu Yang. Physics-informed machine learning. *Nature Reviews Physics*, 3(6):422–440, 2021.
- [13] Aditi Krishnapriyan, Amir Gholami, Shandian Zhe, Robert Kirby, and Michael W Mahoney. Characterizing possible failure modes in physics-informed neural networks. *Advances in neural information processing systems*, 34:26548–26560, 2021.
- [14] William La Cava, Bogdan Burlacu, Marco Virgolin, Michael Kommenda, Patryk Orzechowski, Fabrício Olivetti de França, Ying Jin, and Jason H Moore. Contemporary symbolic regression methods and their relative performance. *Advances in neural information processing systems*, 2021(DB1):1, 2021.
- [15] Jia Li, Ge Li, Yongmin Li, and Zhi Jin. Structured chain-of-thought prompting for code generation. *ACM Transactions on Software Engineering and Methodology*, 34(2):1–23, 2025.
- [16] Lisha Li, Kevin Jamieson, Giulia DeSalvo, Afshin Rostamizadeh, and Ameet Talwalkar. Hyperband: A novel bandit-based approach to hyperparameter optimization. *Journal of Machine Learning Research*, 18(185):1–52, 2018.
- [17] Raymond Li, Loubna Ben Allal, Yangtian Zi, Niklas Muennighoff, Denis Kocetkov, Chenghao Mou, Marc Marone, Christopher Akiki, Jia Li, Jenny Chim, et al. Starcoder: may the source be with you! *arXiv preprint arXiv:2305.06161*, 2023.
- [18] Shanda Li, Tanya Marwah, Junhong Shen, Weiwei Sun, Andrej Risteski, Yiming Yang, and Ameet Talwalkar. Codepde: An inference framework for llm-driven pde solver generation. *arXiv preprint arXiv:2505.08783*, 2025.
- [19] Zongyi Li, Nikola Kovachki, Kamyar Azizzadenesheli, Burigede Liu, Kaushik Bhattacharya, Andrew Stuart, and Anima Anandkumar. Fourier neural operator for parametric partial differential equations. *arXiv preprint arXiv:2010.08895*, 2020.
- [20] Adian Liusie, Vatsal Raina, Yassir Fathullah, and Mark Gales. Efficient llm comparative assessment: a product of experts framework for pairwise comparisons. *arXiv preprint arXiv:2405.05894*, 2024.
- [21] Anton Lozhkov, Raymond Li, Loubna Ben Allal, Federico Cassano, Joel Lamy-Poirier, Nouamane Tazi, Ao Tang, Dmytro Pykhtar, Jiawei Liu, Yuxiang Wei, et al. Starcoder 2 and the stack v2: The next generation. *arXiv preprint arXiv:2402.19173*, 2024.
- [22] Lu Lu, Xuhui Meng, Zhiping Mao, and George Em Karniadakis. Deepxde: A deep learning library for solving differential equations. *SIAM review*, 63(1):208–228, 2021.

- [23] Aman Madaan, Niket Tandon, Prakhar Gupta, Skyler Hallinan, Luyu Gao, Sarah Wiegrefe, Uri Alon, Nouha Dziri, Shrimai Prabhunoye, Yiming Yang, et al. Self-refine: Iterative refinement with self-feedback. *Advances in Neural Information Processing Systems*, 36:46534–46594, 2023.
- [24] Tobias Pfaff, Meire Fortunato, Alvaro Sanchez-Gonzalez, and Peter Battaglia. Learning mesh-based simulation with graph networks. In *International conference on learning representations*, 2020.
- [25] Md Ashiqur Rahman, Robert Joseph George, Mogab Elleithy, Daniel Leibovici, Zongyi Li, Boris Bonev, Colin White, Julius Berner, Raymond A Yeh, Jean Kossaifi, et al. Pretraining codomain attention neural operators for solving multiphysics pdes. *Advances in Neural Information Processing Systems*, 37:104035–104064, 2024.
- [26] Maziar Raissi, Paris Perdikaris, and George E Karniadakis. Physics-informed neural networks: A deep learning framework for solving forward and inverse problems involving nonlinear partial differential equations. *Journal of Computational physics*, 378:686–707, 2019.
- [27] Baptiste Roziere, Jonas Gehring, Fabian Gloeckle, Sten Sootla, Itai Gat, Xiaoqing Ellen Tan, Yossi Adi, Jingyu Liu, Romain Sauvestre, Tal Remez, et al. Code llama: Open foundation models for code. *arXiv preprint arXiv:2308.12950*, 2023.
- [28] Samuel H Rudy, Steven L Brunton, Joshua L Proctor, and J Nathan Kutz. Data-driven discovery of partial differential equations. *Science advances*, 3(4):e1602614, 2017.
- [29] Noah Shinn, Federico Cassano, Ashwin Gopinath, Karthik Narasimhan, and Shunyu Yao. Reflexion: Language agents with verbal reinforcement learning. *Advances in Neural Information Processing Systems*, 36:8634–8652, 2023.
- [30] Khemraj Shukla, Ameya D Jagtap, and George Em Karniadakis. Parallel physics-informed neural networks via domain decomposition. *Journal of Computational Physics*, 447:110683, 2021.
- [31] Vincent Sitzmann, Julien Martel, Alexander Bergman, David Lindell, and Gordon Wetzstein. Implicit neural representations with periodic activation functions. *Advances in neural information processing systems*, 33:7462–7473, 2020.
- [32] Jasper Snoek, Hugo Larochelle, and Ryan P Adams. Practical bayesian optimization of machine learning algorithms. *Advances in neural information processing systems*, 25, 2012.
- [33] Hao Sun, Yunyi Shen, and Jean-Francois Ton. Rethinking bradley-terry models in preference-based reward modeling: Foundations, theory, and alternatives. *arXiv preprint arXiv:2411.04991*, 2024.
- [34] Makoto Takamoto, Timothy Praditia, Raphael Leiteritz, Daniel MacKinlay, Francesco Alesiani, Dirk Pflüger, and Mathias Niepert. Pdebench: An extensive benchmark for scientific machine learning. *Advances in Neural Information Processing Systems*, 35:1596–1611, 2022.
- [35] Hugo Touvron, Louis Martin, Kevin Stone, Peter Albert, Amjad Almahairi, Yasmine Babaei, Nikolay Bashlykov, Soumya Batra, Prajjwal Bhargava, Shruti Bhosale, Dan Bikel, Lukas Blecher, Cristian Canton Ferrer, Moya Chen, Guillem Cucurull, David Esiobu, Jude Fernandes, Jeremy Fu, Wenyin Fu, Brian Fuller, Cynthia Gao, Vedanuj Goswami, Naman Goyal, Anthony Hartshorn, Saghar Hosseini, Rui Hou, Hakan Inan, Marcin Kardas, Viktor Kerkez, Madian Khabsa, Isabel Kloumann, Artem Korenev, Punit Singh Koura, Marie-Anne Lachaux, Thibaut Lavril, Jenya Lee, Diana Liskovich, Yinghai Lu, Yuning Mao, Xavier Martinet, Todor Mihaylov, Pushkar Mishra, Igor Molybog, Yixin Nie, Andrew Poulton, Jeremy Reizenstein, Rashi Rungta, Kalyan Saladi, Alan Schelten, Ruan Silva, Eric Michael Smith, Ranjan Subramanian, Xiaoqing Ellen Tan, Binh Tang, Ross Taylor, Adina Williams, Jian Xiang Kuan, Puxin Xu, Zheng Yan, Iliyan Zarov, Yuchen Zhang, Angela Fan, Melanie Kambadur, Sharan Narang, Aurelien Rodriguez, Robert Stojnic, Sergey Edunov, and Thomas Scialom. Llama 2: Open foundation and fine-tuned chat models, 2023.
- [36] Sifan Wang, Yujun Teng, and Paris Perdikaris. Understanding and mitigating gradient flow pathologies in physics-informed neural networks. *SIAM Journal on Scientific Computing*, 43(5):A3055–A3081, 2021.
- [37] Sifan Wang, Xinling Yu, and Paris Perdikaris. When and why pinns fail to train: A neural tangent kernel perspective. *Journal of Computational Physics*, 449:110768, 2022.
- [38] Xuezhi Wang, Jason Wei, Dale Schuurmans, Quoc V Le, Ed H. Chi, Sharan Narang, Aakanksha Chowdhery, and Denny Zhou. Self-consistency improves chain of thought reasoning in language models. In *The Eleventh International Conference on Learning Representations*, 2023.
- [39] Yicheng Wang, Xiaotian Han, Chia-Yuan Chang, Daochen Zha, Ulisses Braga-Neto, and Xia Hu. Auto-pinn: Understanding and optimizing physics-informed neural architecture, 2023.

- [40] Yifan Wang and Linlin Zhong. Nas-pinn: Neural architecture search-guided physics-informed neural network for solving pdes, 2023.
- [41] Jason Wei, Xuezhi Wang, Dale Schuurmans, Maarten Bosma, brian ichter, Fei Xia, Ed H. Chi, Quoc V Le, and Denny Zhou. Chain of thought prompting elicits reasoning in large language models. In Alice H. Oh, Alekh Agarwal, Danielle Belgrave, and Kyunghyun Cho, editors, *Advances in Neural Information Processing Systems*, 2022.
- [42] Chenxi Wu, Min Zhu, Qinyang Tan, Yadhu Kartha, and Lu Lu. A comprehensive study of non-adaptive and residual-based adaptive sampling for physics-informed neural networks. *Computer Methods in Applied Mechanics and Engineering*, 403:115671, 2023.
- [43] Qingpo Wuwu, Chonghan Gao, Tianyu Chen, Yihang Huang, Yuekai Zhang, Jianing Wang, Jianxin Li, Haoyi Zhou, and Shanghang Zhang. Pinnsagent: Automated pde surrogation with large language models, 2025.
- [44] John Yang, Carlos E Jimenez, Alexander Wettig, Kilian Lieret, Shunyu Yao, Karthik Narasimhan, and Ofir Press. Swe-agent: Agent-computer interfaces enable automated software engineering. *Advances in Neural Information Processing Systems*, 37:50528–50652, 2024.
- [45] Shunyu Yao, Dian Yu, Jeffrey Zhao, Izhak Shafran, Tom Griffiths, Yuan Cao, and Karthik Narasimhan. Tree of thoughts: Deliberate problem solving with large language models. *Advances in neural information processing systems*, 36:11809–11822, 2023.
- [46] Jeremy Yu, Lu Lu, Xuhui Meng, and George Em Karniadakis. Gradient-enhanced physics-informed neural networks for forward and inverse pde problems. *Computer Methods in Applied Mechanics and Engineering*, 393:114823, 2022.
- [47] Richard Zanibbi, Kenny Davila, Andrew Kane, and Frank Wm Tompa. Multi-stage math formula search: Using appearance-based similarity metrics at scale. In *Proceedings of the 39th International ACM SIGIR conference on Research and Development in Information Retrieval*, pages 145–154, 2016.

## APPENDIX

## 1 DETAILS OF KNOWLEDGE-BASED MATCHING IN THE PINN AGENT

In Sec. 4.3 of the main text, we introduced knowledge-based matching, which aligns PDE features with architecture capabilities through a weighted similarity score. This appendix provides the detailed definitions of the PDE feature representation used on the PINN side.

## 1.1 PDE FEATURE REPRESENTATION

Each PDE  $E$  is mapped to a three-dimensional feature vector

$$\phi(E) = [f_{\text{per}}(E), f_{\text{geo}}(E), f_{\text{ms}}(E)]^\top, \quad (1)$$

which captures periodicity, geometry complexity, and multi-scale demand, respectively.

**Periodicity.** The degree of periodicity is quantified as

$$f_{\text{per}}(E) = \frac{|\mathcal{P}(E)|}{d}, \quad (2)$$

where  $d$  denotes the number of spatial dimensions and  $\mathcal{P}(E)$  is the set of spatial axes with periodic boundary conditions. If all spatial directions are periodic then  $|\mathcal{P}(E)| = d$  and  $f_{\text{per}}(E) = 1$ ; if none are periodic then  $|\mathcal{P}(E)| = 0$  and  $f_{\text{per}}(E) = 0$ ; mixed cases lie between 0 and 1.

**Geometry complexity.** Geometry complexity combines the irregularity of the domain shape and the irregularity of the numerical discretization. We first define two scalar scores:  $c_\Omega(E)$  for the domain and  $c_{\text{disc}}(E)$  for the discretization. The domain score  $c_\Omega(E)$  is assigned as 0 for axis-aligned rectangles or boxes, 0.3 for smoothly curved domains, 0.6 for multi-component domains, and 0.9 for highly irregular or fractured geometries. The discretization score  $c_{\text{disc}}(E)$  is set to 0 for Cartesian grids, 0.5 for structured curvilinear grids, and 0.8 for unstructured meshes (e.g., FEM-type discretizations). We then combine these scores as

$$f_{\text{geo}}(E) = \text{clip}(\lambda_\Omega c_\Omega(E) + \lambda_{\text{disc}} c_{\text{disc}}(E), 0, 1), \quad (3)$$

where  $\lambda_\Omega, \lambda_{\text{disc}} \geq 0$  are fixed weights satisfying  $\lambda_\Omega + \lambda_{\text{disc}} = 1$ , and  $\text{clip}(x, 0, 1) = \min(\max(x, 0), 1)$  projects the value into  $[0, 1]$ . In our experiments we use  $\lambda_\Omega = 0.6$  and  $\lambda_{\text{disc}} = 0.4$  and keep them fixed for all PDEs.

**Multi-scale demand.** The multi-scale demand reflects the presence of strong scale separation, nonlinear interactions, or stiff transport phenomena. We construct an intermediate score

$$\tilde{f}_{\text{ms}}(E) = \alpha_1 \mathbf{1}_{\{m(E) \geq 3\}} + \alpha_2 \mathbf{1}_{\{\text{NL}(E)=1\}} + \alpha_3 \log(1 + \text{Re}(E) + \text{Pe}(E)) + \alpha_4 \mathbf{1}_{\{\text{FR}(E)=1\}}, \quad (4)$$

where:

- $m(E)$  is the highest derivative order in the PDE;
- $\text{NL}(E) \in \{0, 1\}$  indicates whether the PDE contains nonlinear terms;
- $\text{Re}(E)$  and  $\text{Pe}(E)$  are Reynolds and Péclet numbers when applicable (set to 0 otherwise);
- $\text{FR}(E) \in \{0, 1\}$  indicates the presence of nonlocal, fractional, or integral operators;
- $\mathbf{1}_{\{\cdot\}}$  is the indicator function.

The final multi-scale feature is normalized into  $[0, 1]$  by a logistic mapping,

$$f_{\text{ms}}(E) = \sigma(\tilde{f}_{\text{ms}}(E)) = \frac{1}{1 + \exp(-\tilde{f}_{\text{ms}}(E))}. \quad (5)$$

We use the fixed weights  $(\alpha_1, \alpha_2, \alpha_3, \alpha_4) = (0.8, 0.8, 0.4, 1.0)$  for all experiments.

## 1.2 PINN ARCHITECTURE CAPABILITY REPRESENTATION

To support automatic and interpretable architecture selection, we represent each PINN architecture  $A$  by a three dimensional capability vector

$$\psi(A) = (a_{\text{per}}(A), a_{\text{geo}}(A), a_{\text{ms}}(A)), \quad (6)$$

where  $a_{\text{per}}(A)$ ,  $a_{\text{geo}}(A)$ , and  $a_{\text{ms}}(A)$  denote the capability of  $A$  on highly periodic, geometrically complex, and strongly multi scale PDEs, respectively. All three entries lie in  $[0, 1]$ , with larger values indicating better

performance on the corresponding class of tasks. This vector is estimated directly from data, using controlled benchmark PDEs and a combination of absolute and relative performance measures.

We consider a collection of benchmark PDE tasks, each denoted by  $E$ . From the previous subsection, each task is associated with a PDE attribute vector  $\phi(E) = (f_{\text{per}}(E), f_{\text{geo}}(E), f_{\text{ms}}(E))$ , where  $f_{\text{per}}(E)$ ,  $f_{\text{geo}}(E)$ , and  $f_{\text{ms}}(E)$  are scalar scores in  $[0, 1]$  that quantify the periodicity, geometry complexity, and multi scale demand of  $E$ . Based on the largest component of  $\phi(E)$ , we assign each task to one of three attribute focused subsets: the high periodicity set  $\mathcal{E}_{\text{per}}$ , the high geometry complexity set  $\mathcal{E}_{\text{geo}}$ , and the high multi scale set  $\mathcal{E}_{\text{ms}}$ .

For each architecture  $A$  (e.g., CNN, MLP, GNN, and Transformer) and task  $E$ , we train a PINN and record a scalar error metric  $y(A, E)$ , e.g., the mean squared PDE residual or the relative  $L^2$  error. The values  $\{y(A, E)\}$  form an architecture–task error matrix that serves as the basis for capability estimation. At a high level, we use this matrix in three steps: 1) we first compute **normalized average scores** for each architecture within each attribute subset, 2) then derive **Bradley–Terry based relative scores** from pairwise win–loss comparisons, and 3) finally **fuse the absolute and relative scores** to obtain the capability vector  $\psi(A)$ .

**Absolute Capability from Normalized Error** For a given attribute, such as periodicity, we first derive an absolute capability estimate from average error. Restricting attention to the high periodicity set  $\mathcal{E}_{\text{per}}$ , we compute the mean error of architecture  $A$  as

$$\bar{y}_{\text{per}}(A) = \frac{1}{|\mathcal{E}_{\text{per}}|} \sum_{E \in \mathcal{E}_{\text{per}}} y(A, E), \quad (7)$$

where  $|\mathcal{E}_{\text{per}}|$  is the number of tasks in this subset and  $\bar{y}_{\text{per}}(A)$  is a scalar summarizing the overall error of  $A$  on periodic tasks. We then apply min–max normalization across architectures,

$$\tilde{y}_{\text{per}}(A) = \frac{\bar{y}_{\text{per}}(A) - \min_{A'} \bar{y}_{\text{per}}(A')}{\max_{A'} \bar{y}_{\text{per}}(A') - \min_{A'} \bar{y}_{\text{per}}(A') + \varepsilon}, \quad (8)$$

where  $\varepsilon$  is a small constant that avoids division by zero. Finally, we convert normalized error into an absolute capability score

$$a_{\text{per}}^{\text{Abs}}(A) = 1 - \tilde{y}_{\text{per}}(A), \quad (9)$$

so that smaller errors correspond to larger capability values in  $[0, 1]$ . The same procedure applied to  $\mathcal{E}_{\text{geo}}$  and  $\mathcal{E}_{\text{ms}}$  yields the absolute geometry and multi scale capability estimates  $a_{\text{geo}}^{\text{Abs}}(A)$  and  $a_{\text{ms}}^{\text{Abs}}(A)$ .

**Relative Capability via Bradley–Terry Model** Absolute errors can be influenced by the overall difficulty of a task subset. To obtain a complementary measure that focuses on relative ordering between architectures, we employ the Bradley–Terry (BT) model (33; 20) on win–loss statistics.

Again considering the high periodicity subset  $\mathcal{E}_{\text{per}}$ , for any pair of architectures  $(A_i, A_j)$  and task  $E \in \mathcal{E}_{\text{per}}$ , we say that  $A_i$  wins over  $A_j$  on  $E$  if

$$y(A_i, E) < y(A_j, E). \quad (10)$$

Aggregating over all tasks in  $\mathcal{E}_{\text{per}}$ , we count the number of wins

$$n_{ij} = \text{number of tasks in } \mathcal{E}_{\text{per}} \text{ where } y(A_i, E) < y(A_j, E), \quad (11)$$

and similarly  $n_{ji}$  for wins of  $A_j$  over  $A_i$ . The collection  $\{n_{ij}\}$  is treated as the observed win–loss data for periodic tasks.

The BT model introduces, for this attribute, a scalar ability parameter  $\theta_{\text{per}}(A)$  for each architecture  $A$ . This parameter is not a neural network weight, but a one dimensional statistical parameter that reflects the overall strength of  $A$  on high periodicity tasks. Under the BT model, the probability that  $A_i$  wins against  $A_j$  in a generic periodic task is

$$p_{ij} = \Pr(A_i \succ A_j) = \frac{\exp(\theta_{\text{per}}(A_i))}{\exp(\theta_{\text{per}}(A_i)) + \exp(\theta_{\text{per}}(A_j))}. \quad (12)$$

Given the observed win counts  $n_{ij}$  and  $n_{ji}$ , the likelihood of these data under the model is

$$L(\theta_{\text{per}}) = \prod_{i < j} p_{ij}^{n_{ij}} (1 - p_{ij})^{n_{ji}}, \quad (13)$$

where the product ranges over all unordered architecture pairs  $(i, j)$  and  $\theta_{\text{per}}$  denotes the collection of all ability parameters. Intuitively,  $L(\theta_{\text{per}})$  is the probability that, if the true win probabilities were given by the BT model with parameters  $\theta_{\text{per}}$ , one would observe exactly the win–loss counts recorded in  $\{n_{ij}\}$ .

We obtain the BT ability parameters by maximizing this likelihood, or equivalently the log likelihood, with respect to  $\theta_{\text{per}}$ . This yields a set of scalar values  $\theta_{\text{per}}^*(A)$ , one for each architecture, that best explains the

observed win–loss data on periodic tasks. To convert these unnormalized abilities into a  $[0, 1]$  scale, we apply min–max normalization

$$a_{\text{per}}^{\text{BT}}(A) = \frac{\theta_{\text{per}}^*(A) - \min_{A'} \theta_{\text{per}}^*(A')}{\max_{A'} \theta_{\text{per}}^*(A') - \min_{A'} \theta_{\text{per}}^*(A') + \varepsilon}. \quad (14)$$

The same BT procedure applied to  $\mathcal{E}_{\text{geo}}$  and  $\mathcal{E}_{\text{ms}}$  produces relative capability scores  $a_{\text{geo}}^{\text{BT}}(A)$  and  $a_{\text{ms}}^{\text{BT}}(A)$  for geometry and multi scale attributes.

**Capability Fusion and Final Representation** For each attribute dimension  $k \in \{\text{per}, \text{geo}, \text{ms}\}$  we now have two capability estimates: an absolute estimate  $a_k^{\text{Abs}}(A)$  derived from normalized average errors, and a relative estimate  $a_k^{\text{BT}}(A)$  derived from win–loss relationships. The two measures capture complementary information: absolute performance level and relative ordering across architectures. We therefore form the final capability entry along dimension  $k$  by a simple linear fusion

$$a_k(A) = \omega_k a_k^{\text{BT}}(A) + (1 - \omega_k) a_k^{\text{Abs}}(A), \quad (15)$$

where  $\omega_k \in [0, 1]$  is a data–driven fusion weight for attribute  $k$ . To determine  $\omega_k$ , we draw bootstrap resamples of the task subset  $\mathcal{E}_k$ , recompute  $a_k^{\text{BT}}(A)$  and  $a_k^{\text{Abs}}(A)$  on each resample, and estimate their empirical variances  $\sigma_{k,\text{BT}}^2$  and  $\sigma_{k,\text{Abs}}^2$ . We then set

$$\omega_k = \frac{\sigma_{k,\text{Abs}}^2}{\sigma_{k,\text{Abs}}^2 + \sigma_{k,\text{BT}}^2}, \quad (16)$$

so that the estimator with smaller variance (more stable across resamples) receives a larger effective weight.

The final architecture capability vector

$$\psi(A) = (a_{\text{per}}(A), a_{\text{geo}}(A), a_{\text{ms}}(A)) \quad (17)$$

is stored in the knowledge base and later matched against PDE attribute vectors  $\phi(E)$  for new tasks. This representation allows the system to reason about architecture–PDE alignment in a quantitative and interpretable manner.

## 2 FEEDBACK AGENT QUALITY METRICS

The validation score produced by the *Feedback Agent* agent aggregates four normalized metrics, each designed to capture a complementary aspect of code quality. Below we detail the first three metrics; the robustness metric is described separately.

**(i) Convergence efficiency.** Convergence efficiency measures how quickly a model reaches a stable solution. We define it based on the number of training steps required for the loss to fall below a pre-specified tolerance  $\tau$ :

$$T_{\text{conv}} = \min\{t \mid L_t \leq \tau\}, \quad m_{\text{conv}} = \frac{1}{T_{\text{conv}}}, \quad (18)$$

where  $L_t$  denotes the training loss at iteration  $t$ . A smaller  $T_{\text{conv}}$  leads to a higher convergence score. For comparability across models, we normalize the score using the range of convergence steps observed in the search space:

$$\hat{m}_{\text{conv}} = \frac{T_{\text{max}} - T_{\text{conv}}}{T_{\text{max}} - T_{\text{min}}}, \quad (19)$$

where  $T_{\text{min}}$  and  $T_{\text{max}}$  denote, respectively, the fastest and slowest convergence times among all candidates. This normalization ensures  $\hat{m}_{\text{conv}} \in [0, 1]$ , with higher values indicating more efficient convergence.

**(ii) Predictive accuracy.** Accuracy is assessed by the discrepancy between the model output and the governing PDE. Specifically, we compute the mean squared error (MSE) of the PDE residual over the training domain:

$$m_{\text{acc}} = -\text{MSE}(\mathcal{N}_\theta, E), \quad (20)$$

where  $\mathcal{N}_\theta$  denotes the physics-informed neural network (PINN) parameterized by  $\theta$ , and  $E$  represents the target PDE operator. The negative sign ensures that lower residual error corresponds to a higher accuracy score.

**(iii) Model complexity.** Complexity reflects the resource demand of the model. We quantify it by the number of trainable parameters (or equivalently the computational cost in FLOPs), normalized with respect to the maximum within the search space:

$$m_{\text{comp}} = \frac{\#\text{Params}(\mathcal{N}_\theta)}{\max \#\text{Params}}, \quad (21)$$

where  $\#\text{Params}(\mathcal{N}_\theta)$  is the parameter count of the candidate PINN and  $\max \#\text{Params}$  is the maximum parameter count among all models considered. A lower value of  $m_{\text{comp}}$  indicates a more compact architecture.

**(iv) Robustness.** We quantify robustness by combining two complementary indicators. The first indicator, *loss smoothness*, measures the stability of the training trajectory. Intuitively, when the loss fluctuates strongly across iterations, the optimization process is less reliable. We capture this by computing the normalized variation of the loss:

$$m_{\text{smooth}} = 1 - \frac{\text{Std}(\Delta L_t)}{\text{Mean}(L_t)}, \quad \Delta L_t = L_t - L_{t-1}, \quad (22)$$

where  $L_t$  denotes the training loss at iteration  $t$ , and  $\Delta L_t$  is the difference between consecutive iterations. A higher value of  $m_{\text{smooth}}$  indicates a smoother and more stable training curve.

The second indicator, *gradient health*, evaluates whether the gradient magnitude remains within a reasonable range, avoiding both vanishing and exploding gradients. Specifically,

$$m_{\text{grad}} = \begin{cases} 1, & \epsilon \leq \frac{\|\nabla_{\theta} L\|}{d} \leq \kappa, \\ 0, & \text{otherwise,} \end{cases} \quad (23)$$

where  $\nabla_{\theta} L$  is the gradient of the loss with respect to the parameters,  $d$  is the number of parameters, and  $\epsilon, \kappa > 0$  are user-defined thresholds specifying the acceptable lower and upper bounds of the normalized gradient magnitude.

Finally, we define the robustness score as a convex combination of the two indicators:

$$m_{\text{rob}} = \alpha m_{\text{smooth}} + (1 - \alpha) m_{\text{grad}}, \quad (24)$$

where  $\alpha \in [0, 1]$  is a weighting factor that balances the contributions of loss smoothness and gradient health. This formulation ensures that robustness reflects both stable optimization dynamics and well-conditioned gradients.

The overall validation score is defined as a weighted combination of the four normalized metrics:

$$S(C) = w_1 \hat{m}_{\text{conv}} + w_2 \hat{m}_{\text{acc}} + w_3 \hat{m}_{\text{comp}} + w_4 \hat{m}_{\text{rob}}, \quad (25)$$

where  $w_1, w_2, w_3, w_4 \geq 0$  are user-specified weights that control the relative importance of convergence efficiency, predictive accuracy, model complexity, and robustness, respectively. By tuning the weights, one can emphasize different aspects of model quality depending on the application.

## 3 EXTENDED RESULTS

### 3.1 MSE AND SUCCESS RATE ACROSS PDE BENCHMARKS

For completeness, we report the full experimental results across all 14 PDE benchmarks. Table 1 presents the mean squared error (MSE) together with standard deviations, complementing the aggregated results in the main text. Table 2 provides per-PDE success rates (%) averaged over 10 runs, offering a more fine-grained view of performance across different equations and dimensions.

**Table 1:** Comparative performance (MSE) of **Lang-PINN** and baseline approaches on 14 different PDEs. Results are averaged over 10 runs.

PDEs	RandomAgent	BayesianAgent	PINNsAgent	PINNacle	SCoT	Self-Debug	Ours
<b>1D</b>							
Burgers	6.63E-02 (±1.10E-01)	8.70E-02 (±6.51E-03)	1.10E-04 (±7.76E-05)	7.90E-05	1.40E+01 (±1.06E+00)	1.26E+01 (±9.54E-01)	6.48E-05 (±9.00E-05)
Wave-C	1.50E-01 (±1.46E-01)	1.78E-01 (±3.84E-02)	3.74E-02 (±4.32E-02)	3.01E-03	1.28E+00 (±6.21E-02)	1.18E+00 (±5.72E-02)	2.25E-03 (±1.80E-04)
KS	1.09E+00 (±3.58E-02)	1.10E+00 (±2.55E-03)	1.09E+00 (±3.20E-02)	1.04E+00	3.33E+00 (±7.80E-02)	2.93E+00 (±6.86E-02)	1.62E-03 (±1.35E-04)
<b>2D</b>							
Burgers-C	2.48E-01 (±4.04E-03)	2.42E-01 (±8.96E-03)	2.93E-01 (±2.43E-02)	1.09E-01	4.54E-01 (±5.57E-02)	4.09E-02 (±5.01E-03)	2.88E-03 (±2.25E-04)
Wave-CG	2.87E-02 (±4.98E-04)	2.11E-02 (±1.12E-02)	4.59E-02 (±1.68E-02)	2.99E-02	2.00E+00 (±1.62E-01)	1.90E+00 (±1.54E-01)	2.52E-03 (±1.62E-04)
Heat-CG	3.96E-01 (±3.22E-01)	1.17E-01 (±3.24E-02)	9.06E-02 (±2.69E-01)	8.53E-04	4.38E+00 (±3.48E-01)	3.81E-02 (±3.03E-03)	1.35E-03 (±9.00E-05)
NS-C	4.02E-03 (±5.93E-03)	5.12E-03 (±1.33E-03)	1.40E-05 (±1.12E-05)	2.33E-05	5.67E-01 (±6.28E-02)	5.27E-01 (±5.84E-02)	4.05E-05 (±4.50E-05)
GS	4.28E-03 (±2.23E-05)	4.03E-03 (±4.47E-04)	3.37E+08 (±1.01E+09)	4.32E-03	3.76E+00 (±5.27E-02)	3.35E+00 (±4.69E-02)	1.89E-03 (±1.44E-04)
Heat-MS	1.84E-02 (±1.18E-02)	7.48E-03 (±3.81E-03)	1.06E-04 (±1.86E-04)	5.27E-05	7.10E-02 (±3.05E-03)	6.04E-03 (±2.59E-04)	2.27E-05 (±7.20E-05)
Heat-VC	3.57E-02 (±8.72E-03)	3.93E-02 (±2.17E-03)	1.43E-02 (±1.77E-02)	1.76E-03	4.46E+00 (±1.05E+00)	4.01E-02 (±9.45E-03)	1.62E-03 (±1.08E-04)
Poisson-MA	5.87E+00 (±1.17E+00)	5.82E+00 (±2.30E+00)	3.16E+00 (±9.92E-01)	1.83E+00	1.24E+04 (±5.71E+03)	1.07E+04 (±4.91E+03)	2.25E-03 (±1.35E-04)
<b>3D</b>							
Poisson-CG	3.82E-02 (±2.15E-02)	2.55E-02 (±5.65E-03)	3.35E-02 (±2.18E-02)	9.51E-04	4.17E-02±3.77E-03	9.51E-03±1.35E-03	1.35E-03 (±9.00E-05)
<b>ND</b>							
Poisson-ND	1.30E-04 (±2.78E-04)	4.72E-05 (±2.76E-06)	4.77E-04 (±3.21E-05)	2.09E-06	9.93E+00 (±6.51E-03)	9.43E+00 (±6.18E-03)	842.00E-06 (±5.17E-07)
Heat-ND	2.58E-00 (±9.87E-02)	1.18E-04 (±8.92E-06)	8.57E-04 (±1.31E-06)	8.52E+00	3.74E+00 (±3.29E-01)	3.40E-03 (±2.99E-04)	4.72E-04 (±6.30E-05)

These results serve as a detailed supplement to the main comparisons: our method consistently achieves the lowest average errors with significantly reduced variance, and obtains higher success rates across nearly all PDEs. In particular, **Lang-PINN** improves code executability and training stability even for challenging high-dimensional and chaotic cases, reinforcing the conclusions drawn in the main paper.

**Table 2:** Success rate (%) of **Lang-PINN** and baseline approaches on 14 different PDEs. Results are averaged over 10 runs.

PDEs	RandomAgent	PINNsAgent	PINNacle	SCoT	Self-Debug	Ours
<b>1D</b>						
Burgers	29.7%	36.2%	38.9%	58.6%	59.7%	84.3%
Wave-C	28.5%	34.8%	37.2%	57.2%	58.3%	80.7%
KS	27.9%	33.5%	35.9%	55.1%	56.4%	82.5%
<b>2D</b>						
Burgers-C	26.1%	33.4%	36.2%	56.3%	58.0%	81.1%
Wave-CG	25.4%	31.2%	34.0%	54.9%	56.1%	77.4%
Heat-CG	25.1%	32.6%	35.1%	55.7%	57.0%	81.6%
NS-C	26.3%	34.1%	36.8%	57.1%	58.9%	83.3%
GS	24.9%	30.7%	33.2%	53.8%	55.0%	78.8%
Heat-MS	26.8%	35.0%	37.6%	58.4%	59.6%	82.7%
Heat-VC	25.6%	32.0%	34.5%	55.2%	56.8%	80.5%
Poisson-MA	23.7%	29.8%	32.7%	52.7%	54.1%	79.2%
<b>3D</b>						
Poisson-CG	22.9%	30.4%	33.5%	53.2%	54.8%	77.9%
<b>ND</b>						
Poisson-ND	21.7%	28.9%	31.7%	51.5%	53.1%	73.3%
Heat-ND	20.9%	29.6%	32.4%	52.1%	53.7%	75.5%

### 3.2 EFFECTIVENESS OF SEMANTIC–SYMBOLIC PDE VERIFICATION

To assess the effectiveness of the proposed semantic–symbolic verification, we perform an evaluation on a held-out collection of PDE tasks. For each task, the LLM generates multiple candidate PDEs. These candidates are grouped into five quality categories based on symbolic correctness (operators, coefficients, and BC/IC structure). For every generated PDE, we compute its semantic consistency score by comparing the model’s natural-language explanation of the equation with the original task description, ensuring that all governing components are aligned.

To measure how well this score reflects actual PDE quality, each candidate PDE is passed through the remaining agents and used to train a PINN, from which we obtain the final mean-squared error. The results in Table 3 show a clear trend: **PDEs with higher semantic consistency yield lower PINN error** (equivalently, larger  $-\log_{10}$ MSE). Across all five quality groups, the semantic score exhibits a strong monotonic relationship with downstream accuracy, with a Pearson correlation of  $r = 0.88$ . These results indicate that semantic–symbolic validation provides a reliable, data-supported proxy for identifying missing constraints and assessing PDE correctness before PINN training.

### 3.3 EFFECTIVENESS OF SEMANTIC–SYMBOLIC PDE VERIFICATION

To assess whether our semantic–symbolic verification reliably reflects PDE quality, we generate multiple PDE candidates for several benchmark tasks and group them into five perturbation classes: C1 (perfect PDE), C2 (notation-level variation), C3 (coefficient error), C4 (missing or incorrect terms), and C5 (structural error or hallucination). For each candidate, we compute the semantic-consistency score and then train a PINN using that PDE to obtain the final  $-\log_{10}$ MSE.

Table 3 shows a clear monotonic trend across all four PDEs: as the perturbation becomes more severe, the semantic score decreases and the resulting PINN error increases. Across the entire evaluation set, the semantic score exhibits a strong negative correlation with the final training error (Pearson correlation  $r = 0.88$ ). These results confirm that the semantic–symbolic metric provides a reliable, data-supported proxy for detecting missing or incorrect constraints prior to PINN training.

### 3.4 SEMANTIC CONSISTENCY THRESHOLDING

To evaluate the reliability of the semantic-consistency metric, we adopt an LLM-as-a-judge procedure. For any pair of textual task descriptions  $d_i$  and  $d_j$ , the judge model is prompted with both descriptions and returns a similarity score  $s \in [0, 1]$ , where larger values indicate stronger semantic alignment.

**Table 3:** Semantic consistency score and PDE MSE loss across five quality levels of LLM-generated PDEs. Categories C1–C5 correspond respectively to: exactly correct PDEs, notation-only variations, coefficient errors, missing/incorrect terms, and structural hallucinations.

PDE Category	Semantic Consistency Score / $-\text{Log}_{10}$ MSE			
	Burgers	Heat-MS	Wave-C	KS
C1 (exactly correct)	1.00 / 4.1884	1.00 / 4.6445	1.00 / 2.6492	1.00 / 2.6055
C2	0.91 / 3.8915	0.89 / 4.3101	0.92 / 2.4302	0.86 / 2.2156
C3	0.71 / 0.6341	0.75 / 0.7478	0.69 / -0.5861	0.70 / -0.8446
C4	0.51 / -0.0546	0.59 / -0.5053	0.45 / -1.5269	0.53 / -1.1914
C5	0.28 / -0.6618	0.23 / -0.8240	0.14 / -2.1447	0.22 / -2.1026
<b>Pearson correlation</b>	<b>0.88</b>			

For threshold calibration, we construct a benchmark containing 200 equivalent pairs and 200 non-equivalent pairs. Each equivalent pair is formed by taking two independently re-expressed descriptions of the same underlying PDE from the Task2PDE dataset. Each non-equivalent pair is formed by taking two descriptions drawn from two different PDEs from Task2PDE dataset.

The score distribution in Fig 1 shows a clear separation. Non-equivalent pairs concentrate below 0.70, while equivalent pairs mostly lie above 0.75, with only a narrow overlap between the two. Based on this separation, we adopt a conservative threshold of 0.80, which retains virtually all equivalent pairs while rejecting nearly all non-equivalent ones. This threshold is used throughout Section 4 to validate LLM-generated PDE formulations.

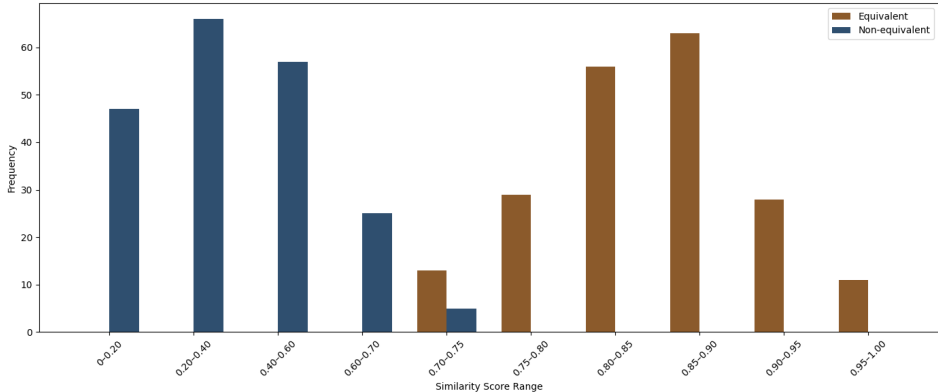


**Figure 1:** Similarity score distribution of 200 equivalent vs. 200 non-equivalent pairs.

### 3.5 END-TO-END WALL-CLOCK TIME EVALUATION

We assess the end-to-end runtime of the full pipeline, measured from pipeline start to until runnable code is produced. In our implementation, the LLM component is accessed through an API (e.g., DeepSeek-V3), and all model computation runs on the provider’s backend. As device-level memory consumption of the LLM is therefore not observable, we focus on **wall-clock time**, which captures the total latency introduced by both LLM inference and subsequent refinement steps.

Each method is executed 10 times under a unified protocol, allowing up to 30 refinement cycles per run. Measured from pipeline start to until runnable code is produced. As shown in Table 4 **Lang-PINN achieves a 21%–52% reduction in total PDE-solving time relative to all baselines**, demonstrating that the proposed multi-agent workflow improves overall efficiency while maintaining solution quality.

**Table 4:** End-to-end wall-clock time, measured from pipeline start until runnable code is produced.

Method	RandomAgent	BayesianAgent	PINNsAgent	SCoT	Self-Debug	Lang-PINN
<b>Avg. Time (s)</b>	413.5	391.2	312.8	291.1	246.4	<b>199.7</b>

### 3.6 THE IMPACT OF THE LLM BACKBONE.

To evaluate how the backbone language model affects Lang-PINN, we run the complete multi-agent workflow with three different LLMs: DeepSeek-V3, Qwen2, and LLaMA2-Chat. All experiments use identical decoding settings and fixed prompt templates. Table 5 shows that although DeepSeek-V3 yields the lowest absolute MSE, Lang-PINN with weaker backbones such as Qwen2 and LLaMA2-Chat still achieves lower error than all baselines that rely on DeepSeek-V3. This indicates that the performance improvement primarily comes from the multi-agent framework, including verification and fallback across the PDE, PINN, Code, and Feedback Agents, rather than from the strength of any specific LLM. A stronger model further improves intermediate reasoning, but the relative gain provided by Lang-PINN remains consistent across all LLM families, showing that the framework generalizes well and is not dependent on a single proprietary backbone.

**Table 5:** Comparison of PINN MSE across different LLM backbones.

PDE	Random	Bayesian	SCoT	Self-Debug	Lang-PINN (DeepSeek-V3)	Lang-PINN (Qwen2)	Lang-PINN (LLaMA2)
KS	1.09E+00	1.10E+00	3.33E+00	2.93E+00	1.62E-03	1.95E-03	2.71E-03
NS-C (2D)	4.02E-03	5.12E-03	5.67E-03	5.27E-01	4.05E-05	5.47E-05	6.88E-05
Poisson-MA	5.87E+00	5.82E+00	1.24E+00	1.07E+00	2.25E-03	2.83E-03	3.22E-03
GS (2D)	4.28E-03	4.03E-03	5.35E-03	5.35E-03	1.89E-03	2.42E-03	3.16E-03

## 4 TASK2PDE DATASET

To rigorously evaluate the ability of language models to map natural-language task descriptions into formal PDE specifications, we construct the **Task2PDE** dataset. The dataset is derived from eight representative PDE families selected from the PINNacle benchmark (7), spanning different spatial dimensions:

- **1D:** Burgers’, Wave–C, Kuramoto–Sivashinsky (KS);
- **2D:** Heat–MS, Poisson–MA, incompressible Navier–Stokes (NS–C);
- **3D:** Poisson–CG;
- **High-dimensional ND:** Heat–ND.

For each PDE family, we construct 50 distinct task descriptions under four difficulty levels, yielding a total of  $8 \times 4 \times 50 = 1600$  samples. Each sample is paired with its ground-truth PDE formulation, including operators, coefficients, boundary/initial conditions, and domain specification. This ensures that every natural-language description corresponds uniquely to one PDE instance, enabling systematic evaluation of semantic-to-symbol grounding.

### 4.1 LINGUISTIC COMPLEXITY LEVELS IN TASK2PDE

For each forward problem in Task2PDE, we construct four task descriptions that all refer to the *same* underlying PDE, but differ in how realistically they reflect human-written text. These four levels are designed to mimic how researchers actually describe PDE-based problems in practice, from clean paper-style statements to noisy, ambiguous, and disorganized notes. In the examples below, we highlight in **bold** the phrases that introduce the level-specific difficulty, and we render each level in a different color for clarity.

#### 4.1.1 LEVEL 1: CLEAN AND EXPLICIT DESCRIPTION.

Level 1 corresponds to a concise and well-structured description, as one would expect in a paper or textbook. The PDE, domain, and boundary/initial conditions are stated explicitly, with no irrelevant or ambiguous information, so the mapping from text to PDE is essentially direct.

Example of Level 1
<p>We consider one-dimensional heat diffusion in a rod of length <math>L = 1</math> with constant thermal conductivity <math>\kappa = 0.01</math>. The temperature <math>u(x, t)</math> satisfies</p> $\partial_t u(x, t) = \kappa \partial_{xx} u(x, t), \quad x \in [0, 1], t > 0.$ <p>Boundary conditions are <math>u(0, t) = 0</math> and <math>u(1, t) = 1</math> for all <math>t &gt; 0</math>, and the initial condition is <math>u(x, 0) = \sin(\pi x)</math>.</p>

In this case, a correct Task2PDE model should recover exactly the ground-truth PDE and its boundary and initial conditions.

#### 4.1.2 LEVEL 2: IRRELEVANT BUT REALISTIC SIDE INFORMATION.

Level 2 keeps the same PDE as Level 1, but mixes in realistically irrelevant details that researchers often include in emails or lab notes, such as comments about the experimental environment or personal impressions. These phrases should not affect the governing equation, yet they increase the risk that an LLM mistakes them for physical conditions.

##### Example of Level 2

We are again simulating heat diffusion in a metal rod of length 1 with constant conductivity  $\kappa = 0.01$  using the standard heat equation on  $[0, 1]$ . **The lab was quite cold in the morning and the left end of the setup felt a bit colder when I touched it, but this is just due to the room air and is not part of the mathematical model.** In the simulation, we still impose  $u(0, t) = 0$  and  $u(1, t) = 1$  for all  $t > 0$ , and use  $u(x, 0) = \sin(\pi x)$  as the initial condition.

The bolded sentences are natural in real experimental notes but do not belong to the PDE constraints. A robust system should ignore these side comments and recover the same PDE and BC/IC as in Level 1; a less robust system may, for example, turn the qualitative remark about “felt a bit colder” into a spurious time-dependent boundary condition.

#### 4.1.3 LEVEL 3: AMBIGUOUS WORDING AND UNDERSPECIFIED TERMINOLOGY.

Level 3 models the situation where the researcher assumes that the reader shares the experimental context, and therefore uses shorthand or ambiguous phrases without fully specifying what they refer to. These expressions are understandable to humans who know the setup, but they can blur the distinction between measurement noise and true physical variation.

##### Example of Level 3

We revisit the same 1D heat conduction setup on  $[0, 1]$  with a homogeneous material. **At the left end, the temperature reading tends to drift over time because the sensor is not very stable, but in the actual experiment the boundary itself is kept at a fixed  $0^\circ\text{C}$  throughout the run.** The right end is maintained at  $1^\circ\text{C}$ , and we use thermal conductivity  $\kappa = 0.01$  with the same sine-shaped initial profile as in our standard diffusion case.

Here, the phrase “**the temperature reading tends to drift over time**” refers to sensor drift rather than a time-varying boundary condition, while the follow-up sentence clarifies that the boundary temperature is fixed. A correct Task2PDE model should resolve this ambiguity and still output  $u(0, t) = 0$  and  $u(1, t) = 1$  as in Level 1. A misinterpreting model may instead treat the drift as a genuine time-dependent boundary, leading to an incorrect PDE–BC pairing.

#### 4.1.4 LEVEL 4: DISORGANIZED, OUT-OF-ORDER DESCRIPTION.

Level 4 reflects free-form lab notebook or chat-style descriptions, where the researcher writes conditions in the order they occur to mind rather than in a structured way. All information needed to reconstruct the same PDE as in Level 1 is present, but it is scattered, partially repeated, and appears in a non-linear order, often mixing preliminary and final settings.

##### Example of Level 4

For this batch of runs we use the same basic heat diffusion setup as before on a rod from  $x = 0$  to  $x = 1$ . **Initially we tried several values for the thermal conductivity, like  $\kappa = 0.005$  and  $\kappa = 0.02$ , but in the final configuration we fixed it at  $\kappa = 0.01$ .** The initial temperature profile is the sine-shaped one from our earlier tests. **The right end is kept at temperature 1 during the whole experiment. At the left end, even though the hardware was moved during calibration and the sensor readings jumped a bit, the boundary itself was maintained at 0 for the entire run.** The evolution of  $u(x, t)$  is still governed by the standard heat equation.

The highlighted phrases illustrate typical disorganization: multiple candidate values of  $\kappa$  appear before the final choice, and the left boundary condition is embedded in comments about hardware motion and sensor jumps. Human readers can usually infer that the true settings are  $\kappa = 0.01$ ,  $u(0, t) = 0$ , and  $u(1, t) = 1$ . An LLM that

fails to integrate these scattered cues may instead latch onto a preliminary  $\kappa$  or ignore the final clarification about the boundary, thus producing an incorrect PDE or boundary conditions even though all necessary information is present in the text.

## 5 PROMPT DESIGN DETAILS OF ALL AGENTS

In this section, we provide the detailed prompts of our all agents, including PDE Agent, PINN Agent, Code Agent, and Feedback Agent.

### 5.1 PDE AGENT

The PDE Agent converts natural-language physical descriptions into multiple plausible governing PDE candidates, expressed in normalized residual form with structured metadata (variables, parameters, domains, and IC/BC).

#### 5.1.1 SYSTEM PROMPT

##### PDE Agent — System Prompt

You are the PDE Agent in a multi-agent PDE-to-PINN system. Your task is to infer plausible governing PDEs from natural-language descriptions of physical systems, without using any ground-truth labels.

You must:

- parse the given physical description  $d$ ;
- reason about the underlying operators, propagation mechanisms, and boundary behavior;
- generate  $K$  independent reasoning trajectories  $\{T_1, \dots, T_K\}$ ;
- in each trajectory, infer exactly ONE plausible PDE candidate  $E_i$ ;
- write the PDE in normalized residual form  $F(u, x, t; \theta) = 0$ ;
- list variables, parameters, and the space-time domain;
- extract initial and boundary conditions when they are implied;
- provide a 24 sentence chain-of-thought explanation for each  $E_i$ ;
- return all trajectories in a single JSON object with the schema:

```
{
  "trajectories": [
    {
      "id": "Ti",
      "reasoning": "<natural-language explanation>",
      "residual_form": "<PDE residual = 0>",
      "variables": "<state and coordinates>",
      "parameters": "<physical parameters>",
      "domain": "<space-time domain>",
      "ic": "<initial condition>",
      "bc": "<boundary condition(s)>"
    },
    ...
  ]
}
```

Follow the JSON schema exactly and do NOT output any text outside JSON.

## 5.1.2 USER PROMPT

**PDE Agent — User Prompt (1D Wave Example)**

Given the following physical description  $d$ , generate  $K = 5$  independent reasoning trajectories  $T_{1:T5}$ . For each trajectory, infer one plausible PDE candidate in residual form  $F(u, x, t; \theta) = 0$ , following the required JSON schema.

[Description  $d$ ]  
 Consider a long, taut string fixed at both ends, positioned horizontally in a controlled laboratory environment. Initially, the string is displaced from its rest position according to a known spatial profile, and it may also possess an initial velocity distribution along its length. Throughout the experiment, the endpoints remain immobile, ensuring that disturbances can only travel along the string. The surrounding air resistance is assumed negligible, so only the inherent properties of the string influence the motion. As time advances, the displacement of each point along the string varies due to the propagation and reflection of waves, potentially creating complex oscillatory patterns. What mathematical equation should be formulated to describe how the vertical displacement of the string at any position changes as a function of both time and spatial coordinate, given the initial shape, initial velocity, and fixed boundary conditions?

Use this description  $d$  to construct 5 reasoning trajectories and output the final result strictly in JSON.

## 5.1.3 ASSISTANT OUTPUT

**PDE Agent — Assistant Output (1D Wave)**

(a) JSON reasoning trajectories:

```

{
  "trajectories": [
    {
      "id": "T1",
      "reasoning": "The description is a textbook setup of a long, taut string with small transverse displacements, fixed at both ends, and negligible air resistance, so the dominant physics is elastic wave propagation along one spatial dimension. For such a uniform string, the balance of transverse forces and inertia leads to the 1D linear wave equation with a constant wave speed determined by string tension and linear density. The fixed endpoints impose zero displacement at both ends of the interval in space. The initial shape and initial velocity translate directly into initial conditions for u and its first time derivative.",
      "residual_form": "F(u,x,t;theta) = u_tt(x,t) - c^2 u_xx(x,t) = 0",
      "variables": "u(x,t): vertical displacement of the string; x: position along the string; t: time.",
      "parameters": "theta = {c, L}, where c > 0 is the constant wave speed (c^2 = T/ with tension T and linear density ) and L is the string length.",
      "domain": "0 < x < L, t > 0.",
      "ic": "u(x,0) = f(x) (given initial shape), u_t(x,0) = g(x) (given initial velocity profile).",
      "bc": "u(0,t) = 0, u(L,t) = 0 for all t 0 (fixed endpoints).",
    },
    {
      "id": "T2",
      "reasoning": "Instead of introducing the wave speed explicitly, we can write the governing law directly from Newtons second law for a small string element. The net transverse force is given by the difference of tensions at its ends, which in the continuous limit produces a term proportional to the second spatial derivative of displacement. Balancing this force with the inertial term involving the linear mass density yields a wave equation with tension and density as the primary parameters.",
      "residual_form": "F(u,x,t;theta) = u_tt(x,t) - T u_xx(x,t) = 0",
      "variables": "u(x,t): vertical displacement; x: coordinate along the string from 0 to L; t: time.",
      "parameters": "theta = {T, , L}, where T > 0 is the constant string tension and > 0 is the constant linear mass density.",
      "domain": "0 < x < L, t > 0.",
      "ic": "u(x,0) = f(x), u_t(x,0) = g(x), where f and g are the prescribed initial displacement and velocity distributions.",
      "bc": "u(0,t) = 0, u(L,t) = 0 for all t 0 (both ends clamped and immobile).",
    },
    .....
  ]
}

```

(b) Canonical PDE after consensus voting (XML form):

```

<root>
  <parsed_pde>u_tt - c^2*u_xx = 0</parsed_pde>
  <variables>u = u(x,t); c = wave speed; x in [0,L]; t >=
    0</variables>
  <domain>x in [0,L], t >= 0</domain>
  <initial_condition>
    u(x,0) = u0(x); u_t(x,0) = v0(x)
  </initial_condition>
  <boundary_condition>
    u(0,t) = 0; u(L,t) = 0 for all t >= 0
  </boundary_condition>
</root>

```

## 5.2 PINN AGENT

The PINN Agent selects the most appropriate PINN architecture for a given PDE, using a combination of physical reasoning, history reuse, knowledge-base capabilities, and feature-capability matching.

### 5.2.1 SYSTEM PROMPT

#### PINN Agent — System Prompt

You are the PINN Architecture Agent in a multi-agent PDE-to-PINN system.

Your role is to determine the most suitable architecture for a given PDE by combining physical reasoning, history reuse (H), knowledge-base capability inference (K), and feature capability matching.

Follow this reasoning workflow:

1. Parse the PDE-XML to identify operators, nonlinearity, IC/BC, geometry, periodicity, and multiscale characteristics.
2. Construct the PDE feature vector  $\phi(E) = [f_{\text{per}}, f_{\text{geo}}, f_{\text{ms}}]_{[0,1]^3}$ .
3. Query the history cache H:
  - Compute semantic similarity between the current PDE and past tasks.
  - If a close match exists, reuse its architecture and hyperparameters.
4. Query knowledge base K:
  - Infer capability vectors  $\psi(A) \in [0.1, 0.9]^3$  for each candidate architecture A {MLP, CNN, GNN, Transformer}.
  - Ground these capabilities in Ks empirical performance and known inductive biases of these architecture families.
5. Perform feature capability matching with weighted cosine similarity:
 
$$S(A|E) = \frac{\langle W \phi(E), \psi(A) \rangle}{(\|W \phi(E)\| * \|\psi(A)\|)}$$
6. Output a JSON object containing history\_match, pde\_features, candidate\_architectures, capability\_vectors, weights, scores, selected, config, backup, and rationale.

Do NOT output text outside JSON.

### 5.2.2 USER PROMPT

#### PINN Agent — User Prompt

Given the PDE-XML, history cache H, and knowledge base K, select the optimal architecture for the task.

Procedure:

- 1) History Reuse:
  - Compare PDE structure + IC/BC + features with entries in H.
  - If similar, directly reuse the stored architecture.
- 2) FeatureCapability Matching:
  - Compute  $\phi(E) \in [0,1]^3$  for periodicity, geometry complexity, and multiscale demand.
  - Infer  $\psi(A)$  for each architecture in: ["MLP", "CNN", "GNN", "Transformer"].
  - Use weights W and compute  $S(A|E)$  for each candidate.
  - Rank and select the best architecture.

Return JSON only:

```
{
  "history_match": {...},
  "pde_features": {...},
  "candidate_architectures": [...],
  "capability_vectors": {...},
  "weights": {...},
  "scores": {...},
  "selected": "...",
  "config": {...},
  "backup": [...],
  "rationale": "..."
}

# PDE-XML:
{pde_xml}
```

### 5.2.3 ASSISTANT OUTPUT

#### Assistant Output

**Example JSON Output:**

```

{
  "history_match": {
    "matched": true,
    "source_task_id": "wave_1d_fixed_ends",
    "reason": "The PDE-XML describes a 1D linear wave
equation  $u_{tt} - c^2 u_{xx} = 0$  on  $x$  in  $[0,L]$  with fixed-end
Dirichlet boundary conditions and prescribed initial
displacement and velocity, which closely matches a
previous wave-string task in H."
  },
  "pde_features": {
    "f_per": 0.1,
    "f_geo": 0.2,
    "f_ms": 0.8
  },
  "candidate_architectures": [
    "MLP", "CNN", "GNN", "Transformer"
  ],
  "capability_vectors": {
    "MLP": [0.2, 0.2, 0.5],
    "CNN": [0.1, 0.6, 0.6],
    "GNN": [0.1, 0.7, 0.4],
    "Transformer": [0.3, 0.4, 0.9]
  },
  "weights": { "f_per": 0.2, "f_geo": 0.2, "f_ms": 0.6 },
  "scores": {
    "MLP": 0.74,
    "CNN": 0.79,
    "GNN": 0.68,
    "Transformer": 0.91
  },
  "selected": "Transformer",
  "config": {
    "d_model": 32,
    "nhead": 2,
    "ffn_hidden": 512,
    "activation": "gelu",
    "sequence_encoding": "space-time tokens with sinusoidal
positional encodings"
  }
}

```

### 5.3 CODE AGENT

The Code Agent takes the analysis XML and PINN architecture templates as input and fills modular code blocks (net, loss, data, train, eval, main) to produce a runnable PINN implementation whose residual is symbolically consistent with the governing PDE.

### 5.3.1 SYSTEM PROMPT

#### Code Agent — System Prompt

You are the Code Agent in a multi-agent PDE-to-PINN system. Your task is to generate fully runnable PINN code blocks from templates and PDE-XML, ensuring that the PDE residual is symbolically equivalent to the governing equation.

You must:

- Generate modular code blocks: [net, loss, data, train, eval, main].
- Preserve all function/class names, signatures, and template structures.
- Fill all placeholders {...} without deleting or renaming supplied templates.
- Implement residual(u, x, t, ...) as a single algebraic expression derived from the PDE-XML using differentiable operators (du\_dx, du\_dt, ...).
- Ensure residual(...) is symbolically equivalent to the PDE (operator level).
- Produce only the completed code blocks no commentary or Markdown fences.
- Never output a full monolithic script; only fill the template blocks.
- main() must only assemble: generate\_data train evaluate.
- Set epochs = 10 unless otherwise specified.

Return ONLY the filled block template.

### 5.3.2 USER PROMPT

#### Code Agent — User Prompt

You are an expert in PINN code generation. Below is the analysis XML (with IC/BC) and the required network implementation.

RULES:

- Generate modular blocks: [net, loss, data, train, eval, main].
- Each block must be fully completed with {} placeholders filled.
- Strictly respect the interface contract implied by the templates:
  - \* net: define class PINN(nn.Module) .....
  - \* loss: define a PINN loss that takes model outputs and data batches.
  - \* data: generate\_data() returns all tensors needed by train/eval.
  - \* train: train(model, data, ...) runs the training loop and returns the model.
  - \* eval: evaluate(model, data, ...) returns metrics.
  - \* main: no new arguments; only wires generate\_data, train, evaluate.
- Do not change function/class names or argument lists in the template.
- No extra explanation, no markdown fences.
- Do NOT generate a monolithic script; only fill the given block template.
- Do not redefine main or PINN outside the provided blocks.

```

- All function/class names must be compatible with the given
  network template.
- For main: do not redefine; only assign hyper-parameters and call
  generate_data, train, evaluate in order.
- Set epochs = 10.
- Implement the PDE residual in a function residual(u, x, t, nu,
  ...)
  that is directly derived from the PDE in the XML, using a single
  algebraic
  expression (with +, -, *, /, ** and derivatives). The residual
  must be
  symbolically equivalent to the PDE so that an external checker
  can parse
  residual(...) back into a symbolic form and verify consistency.

# PDE-XML:
{analysis_xml}

#Templates (MUST MATCH):
{net_template},{loss_template},{data_template},
{train_template},{eval_template},{main_template}

# Block template to fill:
{template}

```

### 5.3.3 ASSISTANT OUTPUT

#### Code Agent — Assistant Output

```

}
import numpy as np
import torch
import torch.nn as nn
# ... (imports, util, PINNsformer definition, etc.)

# ===== net =====
class WavePINNsformer(nn.Module):
    """
    net block
    """
    def __init__(self, d_out=1, d_hidden=512, d_model=32, N=1,
heads=2):
        super().__init__()
        self.model = PINNsformer(
            d_out=d_out,
            d_hidden=d_hidden,
            d_model=d_model,
            N=N,
            heads=heads,
        )

    def forward(self, x, t):

        return self.model(x, t)

def init_weights(m):
    if isinstance(m, nn.Linear):
        torch.nn.init.xavier_uniform_(m.weight)
        if m.bias is not None:
            m.bias.data.fill_(0.01)

```

```

# ===== loss =====
def compute_pde_loss(model, x_res, t_res):
    """
    PDE residual block:  $u_{tt} - 4 u_{xx} = 0$ 
    """
    pred_res = model(x_res, t_res)

    u_x = torch.autograd.grad(
        pred_res, x_res,
        grad_outputs=torch.ones_like(pred_res),
        retain_graph=True, create_graph=True
    )[0]
    u_xx = torch.autograd.grad(
        u_x, x_res,
        grad_outputs=torch.ones_like(pred_res),
        retain_graph=True, create_graph=True
    )[0]

    u_t = torch.autograd.grad(
        pred_res, t_res,
        grad_outputs=torch.ones_like(pred_res),
        retain_graph=True, create_graph=True
    )[0]
    u_tt = torch.autograd.grad(
        u_t, t_res,
        grad_outputs=torch.ones_like(pred_res),
        retain_graph=True, create_graph=True
    )[0]

    # PDE:  $u_{tt} - 4 u_{xx} = 0$ 
    loss_res = torch.mean((u_tt - 4 * u_xx) ** 2)
    return loss_res, pred_res

def compute_bc_loss(model, x_upper, t_upper, x_lower, t_lower):
    """
    Boundary conditions block:
     $u(0, t) = u(1, t) = 0$ 
    """
    pred_upper = model(x_upper, t_upper)
    pred_lower = model(x_lower, t_lower)

    loss_bc = torch.mean(pred_upper ** 2) + torch.mean(pred_lower
    ** 2)
    return loss_bc, pred_upper, pred_lower

def compute_ic_loss(model, x_left, t_left, pi):
    """
    Initial conditions block:
    IC1:  $u(x, 0) = \sin(\pi x) + 0.5 \sin(3 \pi x)$ 
    IC2:  $u_t(x, 0) = 0$ 
    """
    pred_left = model(x_left, t_left)

    #  $u_t(x, 0)$ 
    u_t_left = torch.autograd.grad(
        pred_left, t_left,
        grad_outputs=torch.ones_like(pred_left),
        retain_graph=True, create_graph=True
    )[0]

```

```

# t = 0
u0_pred = pred_left[:, 0] # [N, 1] -> [N]
x0 = x_left[:, 0]

u0_true = torch.sin(pi * x0) + 0.5 * torch.sin(3 * pi * x0)
loss_ic_1 = torch.mean((u0_pred - u0_true) ** 2)
loss_ic_2 = torch.mean(u_t_left ** 2)

loss_ic = loss_ic_1 + loss_ic_2
return loss_ic, pred_left, u_t_left

def compute_total_loss(model, batch, pi, loss_track=None):
    """
        L_total = L_res + L_bc + L_ic
    """
    x_res, t_res = batch["x_res"], batch["t_res"]
    x_left, t_left = batch["x_left"], batch["t_left"]
    x_right, t_right = batch["x_right"], batch["t_right"]
    x_upper, t_upper = batch["x_upper"], batch["t_upper"]
    x_lower, t_lower = batch["x_lower"], batch["t_lower"]

    loss_res, _ = compute_pde_loss(model, x_res, t_res)
    loss_bc, _, _ = compute_bc_loss(model, x_upper, t_upper,
    x_lower, t_lower)
    loss_ic, _, _ = compute_ic_loss(model, x_left, t_left, pi)

    total_loss = loss_res + loss_bc + loss_ic

    if loss_track is not None:
        loss_track.append([
            loss_res.item(),
            loss_ic.item(),
            loss_bc.item()
        ])

    return total_loss, loss_res, loss_ic, loss_bc

# ===== data / train / eval / main
# =====

# - build_dataset(...)
# - train(...)
# - u_analytic(...), evaluate_and_plot(...)
# - main()

...

```

#### 5.4 FEEDBACK AGENT

The Feedback Agent executes the code produced by the Code Agent, extracts runtime and numerical signals, and decides whether the pipeline is valid, faulty, or requires refinement, routing structured instructions back to the appropriate agent.

## 5.4.1 SYSTEM PROMPT

**Feedback Agent — System Prompt**

```

You are the FEEDBACK AGENT in a modular PDE-to-PINN system.

Your responsibility is to:
- execute the code file produced by the Code Agent,
- extract runtime signals,
- evaluate the numerical behavior using standardized metrics,
- determine whether the pipeline is VALID, FAULTY, or REQUIRES
  REFINEMENT,
- and route actionable instructions to the appropriate agent.

RUNTIME RESPONSIBILITIES

1. Execute the generated script inside a controlled sandbox.
2. Capture:
  - stdout
  - stderr (full traceback)
  - return code
  - runtime warnings
3. Detect failure conditions:
  - SyntaxError / ImportError
  - shape/type errors
  - divergence: NaN/Inf in losses, exploding gradients
  - runtime timeout
  - missing outputs

METRIC EXTRACTION

If execution succeeds, normalize four metrics into [0,1]:
- m_conv : convergence efficiency (speed of loss reduction)
- m_acc  : accuracy (PDE residual or RelL2)
- m_comp : model complexity (params/FLOPs inversely mapped)
- m_rob  : robustness (gradient stability, smoothness)

Aggregate:
  S(C) = w1*m_conv + w2*m_acc + w3*m_comp + w4*m_rob

ROUTING LOGIC

If status = FAIL:
  - identify the faulty block {net, loss, data, train, eval,
    main}
  - return an instruction for Code Agent with:
    block_name, error_summary, log_path

If status = SUCCESS but S(C) < threshold:
  - return refinement request (hyperparameter retuning or
    architecture reconsideration) for PINN Agent.

Output MUST be a JSON object.
NO additional text is allowed.

```

## 5.4.2 USER PROMPT

**Feedback Agent — User Prompt**

Evaluate the generated PINN code.

Steps:

- 1) Save the received code into:  
    pinn\_eval.py
- 2) Run with:  
    subprocess.check\_output(..., timeout=120)
- 3) If execution FAILS:
  - capture stderr (string)
  - save full logs to logs/pinn\_eval\_\*.log
  - analyze traceback to localize the faulty block:  
    ["net", "loss", "data", "train", "eval", "main"]
  - return:
 

```
{
            "status": "FAIL",
            "metrics": null,
            "score": null,
            "error_block": "...",
            "error_summary": "...",
            "log_path": "...",
            "action": "call CodeAgent with error_block, log_path,
error_summary"
          }
```
- 4) If execution SUCCEEDS:
  - extract metrics:
 

```
{
            "m_conv": float,
            "m_acc": float,
            "m_comp": float,
            "m_rob": float
          }
```
  - compute S(C)
  - if S(C) >= threshold:
 

```
return {
            "status": "SUCCESS",
            "metrics": {...},
            "score": S,
            "action": "accept"
          }
```
  - else:
 

```
return {
            "status": "SUCCESS",
            "metrics": {...},
            "score": S,
            "action": "request PINNAgent refinement"
          }
```

Output MUST be valid JSON.

### 5.4.3 ASSISTANT OUTPUT

#### Feedback Agent — Assistant Output

```
{
  "status": "SUCCESS",
  "metrics": {
    "m_conv": 0.87,
    "m_acc": 0.82,
    "m_comp": 0.91,
    "m_rob": 0.88
  },
  "score": 0.87,
  "error_block": null,
  "error_summary": null,
  "log_path": "logs/pinn_eval.log",
  "action": "accept"
}
```